Probability distributions for dynamic and extreme responses of linear elastic structures under quasi-stationary harmonizable loads

Zifeng Huang[a,*] and Michael Beer[a, b, c]

[a]*Institute for Risk and Reliability, Leibniz Universiy Hannover, Callinstr. 34, Hannover 30167, Germany*

[b]*Institute for Risk and Uncertainty, University of Liverpool, Peach Street, Liverpool L69 7ZF, United Kingdom*

[c]*International Joint Research Center for Resilient Infrastructure & International Joint Research Center for Engineering Reliability and Stochastic Mechanics, Tongji University, Shanghai 200092, PR China*

Abstract: The non-stationary load models based on the evolutionary power spectral density (EPSD) may lead to ambiguous structural responses. Quasi-stationary harmonizable processes with non-negative Wigner-Ville spectra are suitable for modeling non-stationary loads and analyzing their induced structural responses. In this study, random environmental loads are modeled as quasi-stationary harmonizable processes. The Loève spectrum of a harmonizable load process contains several random physical parameters. An explicit approach to calculate the probability distributions for the dynamic and extreme responses of a linear elastic structure subjected to a quasi-stationary harmonizable load is proposed. Conditioned on the specific values of the load spectral parameters, the harmonizable load process is assumed to be Gaussian. The conditional joint probability density function (PDF) of structural dynamic responses at any finite time instants and the conditional cumulative distribution function (CDF) of the structural extreme response are provided. By multiplying these two conditional probability distributions with the joint PDF of the load spectral parameters, and then integrating these two products over the parameter sample space, the joint PDF of structural dynamic responses at any finite time instants and the CDF of the structural extreme response can be calculated. The efficacy of the proposed approach is numerically validated using two linear elastic systems, which are subjected to non-stationary and non-Gaussian wind and seismic loads, respectively. The merit of the harmonizable load process model is highlighted through a comparative

*Corresponding author

Email address: zifeng.huang@irz.uni-hannover.de (Zifeng Huang) and beer@irz.uni-hannover.de (Michael Beer);

Abbreviations: 1D = one-dimensional; 2D = two-dimensional; 2-DOF = 2-degree-of-freedom; CDF = cumulative distribution function; EPSD = evolutionary power spectral density; MDOF = multi-degree-of-freedom; PDF= probability density function; WVS = Wigner-Ville spectrum; SRD = square root decomposition.

analysis with the EPSD load model.

Keywords: Quasi-stationary harmonizable load process; Joint probability density function; Extreme value distribution; Linear elastic structure.

1. Introduction

Random environmental loads, including extreme wind events and earthquake ground motion, exhibit obvious time-varying properties and thus are usually modeled as non-stationary processes. Due to its ability to physically interpret the local power-frequency distribution at each time instant, the evolutionary power spectral density (EPSD) [1, 2] has wide application in the characterization and simulation of non-stationary earthquake ground motions [3-5] and non-stationary wind speeds [6-9], and the prediction of structural responses [7, 10-14]. Though popular, EPSD has one essential deficiency. For a multi-variate non-stationary load process with time-varying coherences, calculating its correlation functions and the correlation functions of its induced structural responses involves a step of decomposing the load EPSD matrix. When different decomposition methods, e.g., Cholesky decomposition [3], proper orthogonal decomposition [15], or square root decomposition (SRD) [16], are employed, it has been theoretically proven that the obtained load and response correlation functions may be not unique [16].

The harmonizable process [17, 18] considering the spectral correlation represents a natural expansion of the wide-sense stationary process. Its Wigner-Ville spectrum (WVS) characterizes the time-frequency properties and the dual-frequency Loève spectrum describes the spectral correlation. For a harmonizable process, its WVS, Loève spectrum, and correlation function can be uniquely converted to each other by one-dimensional (1D) or two-dimensional (2D) Fourier transform [19, 20]. Thus, the harmonizable process does not suffer from the problem of ambiguous correlation functions, which is encountered by the EPSD model. Similar to the semi-stationary processes characterized by slowly-varying ESPDs [1], the non-negative slowly-varying WVSes of the quasi-stationary harmonizable processes [21] are suitable for characterizing the time-frequency properties of non-stationary loads. A multi-taper S-transform method for the WVS and Loève spectrum estimation has been proposed to estimate the WVSes and Loève spectra of environmental loads based on field-measured records [22]. Applying a quasi-stationary harmonizable load process to a linear elastic structure, it is convenient to calculate the Loève spectrum of the structural response directly by multiplying the load Loève spectrum with the structural frequency response function [23]. Thus, the quasi-stationary harmonizable processes are suitable for characterizing non-stationary loads and analyzing their induced structural responses. Nonetheless, current research regarding the modeling of random loads and structural response analysis based on the quasi-stationary harmonizable process remains relatively limited. In [24, 25], the earthquake ground motion acceleration is modeled as a sigma oscillatory process characterized by its EPSD. The correlation function of the earthquake ground motion, which is calculated from its EPSD, is converted to a Loève spectrum to calculate the structural response Loève spectrum and the response correlation function. Although the Loève spectrum is employed, the structural response analysis under the stochastic seismic load in [24, 25] still remains within the framework of EPSD and thus may suffer from the ambiguity of correlation functions. In [23], two approximate representations of harmonizable processes based on the discrete Fourier transform were proposed to model various non-Gaussian and non-stationary load processes. The joint probability density function (PDF) of the load Fourier coefficients, which can be directly estimated from field-measured load records, is suitable for characterizing the complete probabilistic information of the load processes. The two load representations can be employed to compute the joint PDF of responses at any finite time instants for linear elastic structures. In [26], one of the two load representations based on the discrete Fourier transform has been utilized to model the complete probabilistic information of a fluctuating wind speed process with field-measured wind speed time records. Notably, the joint PDF of a total of 1198 wind speed frequency components was successfully modeled by the D-vine copula distribution. Though versatile for modeling the complete probabilistic information of various random loads, the high dimension of the frequency components may render the evaluation of their joint PDF computationally expensive. The load modeling and response analysis within the framework of the harmonizable process is still an open challenge.

Utilizing the load spectrum containing several random physical parameters proves to be a convenient and practical approach for describing the probabilistic information of environmental loads [27-29]. In this study, random environmental loads are modeled as quasi-stationary harmonizable processes and the Loève spectrum of a harmonizable load process contains several random physical parameters. An explicit approach to calculate dynamic and extreme response probability distributions for a linear elastic structure subjected to a quasi-stationary harmonizable load process is proposed. First, conditioned on the specific values of the load spectral parameters, the harmonizable load process is assumed to be Gaussian. Under this condition, the load Loève spectrum is a deterministic spectrum function and structural response correlation functions can be readily calculated from the deterministic load Loève spectrum. Subsequently, the conditional joint PDF of structural dynamic responses at any finite time instants, and the conditional cumulative distribution function (CDF) of the structural extreme response, conditioned on the values of the load spectral parameters, can be expressed in terms of the response correlation functions. Finally, by multiplying the conditional joint PDF of dynamic responses and the conditional CDF of the extreme response with the joint PDF of the load spectral parameters, and then integrating these two products over the parameter sample space, the joint PDF of structural dynamic responses at any finite time instants and the CDF of the structural extreme response can be calculated.

The remainder of this paper is organized as follows. First, the mathematical definition and properties of the quasi-stationary harmonizable processes, along with the physical interpretation of WVS, are briefly introduced. Subsequently, the proposed approach to calculate dynamic and extreme response probability distributions for linear elastic structures subjected to quasi-stationary harmonizable load processes is provided. Finally, the efficacy of the proposed approach is numerically validated using two multi-degree-of-freedom (MDOF) systems, which are subjected to non-stationary and non-Gaussian wind and seismic loads, respectively. Using the system subjected to a bivariate non-stationary wind speed process with a time-varying coherence, the merit of the harmonizable load process model is highlighted through a comparative analysis with the EPSD load model.

2. Quasi-stationary harmonizable load process

In this section, the mathematical definition of the harmonizable process, along with its correlation function, WVS, and Loève spectrum, is briefly introduced. Subsequently, the quasi-stationarity of the harmonizable process and the physical interpretation of the WVS of the quasi-stationary harmonizable process are provided. A comprehensive introduction to the harmonizable process, along with a theoretical comparative analysis against the semi-stationary process characterized by EPSD, can be found in [20].

A zero-mean, second-order, and real-valued multi-variate harmonizable process $\mathbf{F}(t) = [F_1(t), F_2(t),\ldots, F_{N_\mathbf{F}}(t)]^\mathrm{T}$ is defined as [18, 23]

$$\mathbf{F}(t) = \int_{-\infty}^{+\infty} e^{\mathrm{i}2\pi ft} \mathrm{d}\mathbf{Z}(f), \tag{1}$$

where T is the transposition operator; $\mathbf{Z}(f) = [Z_1(f), Z_2(f),\ldots, Z_{N_\mathbf{F}}(f)]^\mathrm{T}$ is a complex-valued zero-mean process satisfying

$$\mathrm{d}\mathbf{Z}^*(f) = \mathrm{d}\mathbf{Z}(-f); \tag{2}$$

and * is the conjugate operator.

The Loève spectrum of $\mathbf{F}(t)$ is defined as [17]

$$\mathbf{S}_\mathbf{F}(f_1, f_2) = \mathrm{E}\left[\mathrm{d}\mathbf{Z}^*(f_1)\mathrm{d}\mathbf{Z}^\mathrm{T}(f_2)\right] \big/ \mathrm{d}f_1\mathrm{d}f_2, \tag{3}$$

where E[•] is the expectation operator. $\mathbf{S}_\mathbf{F}(f_1, f_2)$ can be continuous functions or the generalized functions consisting of the Dirac delta function $\delta(\bullet)$ [30]. It satisfies

$$\mathbf{S}^*_\mathbf{F}(f_1, f_2) = \mathbf{S}^\mathrm{T}_\mathbf{F}(f_2, f_1). \tag{4}$$

$\mathbf{S}_\mathbf{F}(f_1, f_2)$ and the correlation $\mathbf{R}_\mathbf{F}(t_1, t_2) = \mathrm{E}[\mathbf{F}^*(t_1)\,\mathbf{F}^\mathrm{T}(t_2)]$ of $\mathbf{F}(t)$ constitutes a 2D Fourier transform pair, as illustrated by

$$\mathbf{R}_\mathbf{F}(t_1, t_2) = \int_{-\infty}^{+\infty}\int_{-\infty}^{+\infty} e^{\mathrm{i}2\pi(f_2t_2 - f_1t_1)} \mathbf{S}_\mathbf{F}(f_1, f_2)\mathrm{d}f_1\mathrm{d}f_2 \tag{5}$$

and

$$\mathbf{S}_\mathbf{F}(f_1, f_2) = \int_{-\infty}^{+\infty}\int_{-\infty}^{+\infty} e^{\mathrm{i}2\pi(f_1t_1 - f_2t_2)} \mathbf{R}_\mathbf{F}(t_1, t_2)\mathrm{d}t_1\mathrm{d}t_2. \tag{6}$$

Rotating the time coordinate in $\mathbf{R}_\mathbf{F}(t_1, t_2)$ and the frequency coordinate in $\mathbf{S}_\mathbf{F}(f_1, f_2)$ by 45°, respectively, that is $t = 0.5(t_1 + t_2)$ and $\tau = (t_2 - t_1)$, $f = 0.5(f_1 + f_2)$ and $\xi = (f_2 - f_1)$, $\tilde{\mathbf{R}}_\mathbf{F}(t, \tau) = \mathbf{R}_\mathbf{F}(t - 0.5\tau, t + 0.5\tau)$ and $\tilde{\mathbf{S}}_\mathbf{F}(f, \xi) = \mathbf{S}_\mathbf{F}(f - 0.5\xi, f + 0.5\xi)$ are obtained. $\tilde{\mathbf{R}}_\mathbf{F}(t, \tau)$ and $\tilde{\mathbf{S}}_\mathbf{F}(f, \xi)$ are equivalent to $\mathbf{R}_\mathbf{F}(t_1, t_2)$ and $\mathbf{S}_\mathbf{F}(f_1, f_2)$, respectively, and they can be interchangeably used. The WVS $\mathbf{W}_\mathbf{F}(t, f)$ of $\mathbf{F}(t)$ is defined as [31]

$$\mathbf{W}_{\mathbf{F}}(t,f)=\int_{-\infty}^{+\infty}e^{-\mathrm{i}2\pi f\tau}\tilde{\mathbf{R}}_{\mathbf{F}}(t,\tau)\mathrm{d}\tau, \tag{7}$$

and can also be calculated from $\tilde{\mathbf{S}}_{\mathbf{F}}(f,\xi)$

$$\mathbf{W}_{\mathbf{F}}(t,f)=\int_{-\infty}^{+\infty}e^{\mathrm{i}2\pi\xi t}\tilde{\mathbf{S}}_{\mathbf{F}}(f,\xi)\mathrm{d}\xi. \tag{8}$$

$\mathbf{W}_{\mathbf{F}}(t,f)$ represents the time-frequency property of $\mathbf{F}(t)$. Eqs. (5)-(8) indicate that $\mathbf{R}_{\mathbf{F}}(t_1, t_2)$, $\mathbf{W}_{\mathbf{F}}(t, f)$, and $\mathbf{S}_{\mathbf{F}}(f_1, f_2)$ are in one-to-one correspondence and can be converted to each other by a 1D or 2D Fourier transform [19, 20].

As illustrated in Eq. (1), the definition of the harmonizable process is in the form of the Fourier transform. Any process, that can be expressed in this form, belongs to the class of harmonizable processes. The commonly-used semi-stationary processes characterized by the EPSD [1] and the wavelet processes characterized by the wavelet spectrum [32, 33] can be expressed in the form of Eq. (1), and they both belong to the class of harmonizable processes.

In this study, two assumptions are enforced to $\mathbf{F}(t)$. One is that $\mathbf{F}(t)$ is assumed to be quasi-stationary, that is $\tilde{\mathbf{R}}_{\mathbf{F}}(t, \tau)$ is slowly-varying with respect to t [21, 22]. The specific mathematical definition of the quasi-stationarity of the harmonizable process was provided in [21]. The other one is that the auto-WVSes of $\mathbf{F}(t)$ are non-negative. The conditions for the positive WVSes of harmonizable processes has been investigated in [34].

The physical interpretation of the WVS of the quasi-stationary harmonizable process is provided here. Noting that $\tilde{\mathbf{R}}_{\mathbf{F}}(t, \tau) = \mathbf{R}_{\mathbf{F}}(t-0.5\tau, t+0.5\tau) = \mathrm{E}[\mathbf{F}^*(t-0.5\tau)\,\mathbf{F}^{\mathrm{T}}(t+0.5\tau)]$, from Eq. (7), the WVS $\mathbf{W}_{\mathbf{F}}(t,f)$ of $\mathbf{F}(t)$ can be expressed as

$$\mathbf{W}_{\mathbf{F}}(t,f)=\int_{-\infty}^{+\infty}e^{-\mathrm{i}2\pi f\tau}\mathbf{R}_{\mathbf{F}}(t-0.5\tau,t+0.5\tau)\mathrm{d}\tau=\int_{-\infty}^{+\infty}e^{-\mathrm{i}2\pi f\tau}\mathrm{E}\left[\mathbf{F}^*(t-0.5\tau)\mathbf{F}^{\mathrm{T}}(t+0.5\tau)\right]\mathrm{d}\tau. \tag{9}$$

Eq. (9) indicates that at each time instant t, $\mathbf{W}_{\mathbf{F}}(t,f)$ is the Fourier transform of the correlation function $\mathbf{R}_{\mathbf{F}}(t-0.5\tau, t+0.5\tau)$ of $\mathbf{F}(t)$ around t. Since the correlation function $\mathbf{R}_{\mathbf{F}}(t-0.5\tau, t+0.5\tau)$ of the quasi-stationary $\mathbf{F}(t)$ is slowly-varying with respect to t, in the neighborhood of each time instant t, $\mathbf{R}_{\mathbf{F}}(t-0.5\tau, t+0.5\tau)$ can be regarded as a stationary correlation function, and $\mathbf{W}_{\mathbf{F}}(t,f)$ is just the power spectral density of the stationary correlation function at each time instant t. When $\mathbf{F}(t)$ is a wide-sense stationary process, $\mathbf{W}_{\mathbf{F}}(t,f)$ degenerates to the stationary power spectral density of $\mathbf{F}(t)$. Besides, $\mathbf{W}_{\mathbf{F}}(t,f)$ satisfies the condition that

$$\mathrm{Var}[\mathbf{F}(t)] = \mathbf{R}_{\mathbf{F}}(t,t) = \int_{-\infty}^{+\infty} \mathbf{W}_{\mathbf{F}}(t,f)\mathrm{d}f, \tag{10}$$

where Var[•] is the variance operator. Thus, for a quasi-stationary $\mathbf{F}(t)$, $\mathbf{W}_{\mathbf{F}}(t, f)$ is a time-varying spectrum representing the energy distribution of $\mathbf{F}(t)$ over the time-frequency domain. The WVS of the quasi-stationary harmonizable process shares a similar physical interpretation with that of EPSD.

3. Probability distributions of responses for linear elastic structures

In this section, the calculation of the response correlation function, WVS, and Loève spectrum of an MDOF linear elastic structure subjected to a harmonizable load process is first introduced. Subsequently, the proposed methods to calculate the joint PDF of structural dynamic responses at multiple time instants and the CDF of the structural extreme response are presented in Sections 3.1 and 3.2, respectively.

The differential equation for a MDOF linear elastic structure on a time interval [0, +∞) is

$$\mathbf{M}\ddot{\mathbf{U}}(t) + \mathbf{C}\dot{\mathbf{U}}(t) + \mathbf{K}\mathbf{U}(t) = \mathbf{F}(t,\mathbf{\Theta}), \tag{11}$$

where $\mathbf{M}$, $\mathbf{C}$, and $\mathbf{K}$ are the mass, damping and stiffness matrixes, respectively; $\mathbf{U}(t)$ is an $N_{\mathbf{U}}$-dimensional process representing the structural displacement response; $\dot{}$ and $\ddot{}$ are the first- and second-order derivative operators with respect to t, respectively; $\mathbf{F}(t, \mathbf{\Theta})$ is an $N_{\mathbf{U}}$-dimensional quasi-stationary harmonizable load process defined by Eq. (1); and $\mathbf{\Theta} = [\Theta_1, \Theta_2,\ldots, \Theta_{N_\Theta}]$ is a stochastic vector representing a set of random physical parameters characterizing the randomness of the load Loève spectrum $\mathbf{S}_{\mathbf{F}}(f_1, f_2, \mathbf{\Theta})$. In this study, it is assumed that $\mathbf{U}(t)$ satisfies the initial conditions $\mathbf{U}(0) = \dot{\mathbf{U}}(0) = \mathbf{0}$.

Given a realization $\mathbf{\theta} = [\theta_1, \theta_2,\ldots, \theta_{N_\Theta}]$ of $\mathbf{\Theta}$, the load Loève spectrum $\mathbf{S}_{\mathbf{F}}(f_1, f_2, \mathbf{\theta})$ on this condition becomes a deterministic spectrum function. The conditional probability distribution of the load $\mathbf{F}(t, \mathbf{\theta})$ on the condition of the deterministic $\mathbf{S}_{\mathbf{F}}(f_1, f_2, \mathbf{\theta})$ is assumed to be Gaussian. The rationale for the assumption that $\mathbf{F}(t, \mathbf{\theta})$ is Gaussian on the condition of a realization $\mathbf{\theta}$ of $\mathbf{\Theta}$ is explained here. Simulated records from the commonly-used stochastic process simulation methods based on either the decomposition of the spectrum matrix [3, 35, 36] or the correlation function matrix [15] are Gaussian.

In addition, following the central limit theorem, a linear combination of a set of basis functions with independent stochastic coefficients is approximately a Gaussian process without requiring the same marginal probability distributions of the coefficients [37]. The conditional probability distribution of $\mathbf{F}(t, \boldsymbol{\theta})$ under this assumption is consistent with that of its realizations simulated using the commonly-used simulation methods. Under this assumption, the response $\mathbf{U}(t)$ caused by $\mathbf{F}(t, \boldsymbol{\theta})$ is also Gaussian.

The Loève spectrum $\mathbf{S}_{\mathbf{U}}(f_1, f_2, \boldsymbol{\theta})$ of $\mathbf{U}$(t) caused by $\mathbf{F}(t, \boldsymbol{\theta})$ can be directly calculated from $\mathbf{S}_{\mathbf{F}}(f_1,$ $f_2, \boldsymbol{\theta})$

$$\mathbf{S}_{\mathrm{U}}(f_1, f_2, \boldsymbol{\theta}) = \mathbf{H}^*(f_1)\mathbf{S}_{\mathbf{F}}(f_1, f_2, \boldsymbol{\theta})\mathbf{H}^{\mathrm{T}}(f_2), \tag{12}$$

where $\mathbf{H}(f)$ is the frequency response function matrix of the linear elastic system in Eq. (11)

$$\mathbf{H}(f) = \left[-4\pi^2 f^2\mathbf{M} + \mathrm{i}2\pi f\mathbf{C} + \mathbf{K}\right]^{-1}. \tag{13}$$

The correlation function $\mathbf{R}_{\mathbf{U}}^{(p)(q)}(t_1, t_2, \boldsymbol{\theta})$ can be calculated from $\mathbf{S}_{\mathbf{U}}(f_1, f_2, \boldsymbol{\theta})$

$$\begin{aligned}\mathbf{R}_{\mathrm{U}}^{(p)(q)}(t_1, t_2, \boldsymbol{\theta}) &= \mathrm{E}\left[\frac{\mathrm{d}^p\mathbf{U}^*(t_1)}{\mathrm{d}t_1^p}\frac{\mathrm{d}^q\mathbf{U}^{\mathrm{T}}(t_2)}{\mathrm{d}t_2^q}\right] \\ &= (-\mathrm{i}2\pi)^p(\mathrm{i}2\pi)^q\int_{-\infty}^{+\infty}\int_{-\infty}^{+\infty} e^{\mathrm{i}2\pi(f_2t_2 - f_1t_1)} f_1^p f_2^q \mathbf{S}_{\mathrm{U}}(f_1, f_2, \boldsymbol{\theta})\mathrm{d}f_1\mathrm{d}f_2,\end{aligned} \tag{14}$$

where p and q are non-negative integers. The WVS $\mathbf{W}_{\mathbf{U}}(t, f, \boldsymbol{\theta})$ of $\mathbf{U}(t)$ can be calculated as

$$\mathbf{W}_{\mathrm{U}}(t, f, \boldsymbol{\theta}) = \int_{-\infty}^{+\infty} e^{\mathrm{i}2\pi\xi t}\tilde{\mathbf{S}}_{\mathrm{U}}(f, \xi, \boldsymbol{\theta})\mathrm{d}\xi, \tag{15}$$

where $\tilde{\mathbf{S}}_{\mathbf{U}}(f, \xi, \boldsymbol{\theta}) = \mathbf{S}_{\mathbf{U}}(f - 0.5\xi, f + 0.5\xi, \boldsymbol{\theta})$.

3.1. Joint PDF of structural dynamic responses at multiple time instants

Given finite time instants, $\mathbf{t} = [t_1, t_2, \ldots, t_{N_{\mathbf{t}}}]$, at each time instant t_i, $i = 1, 2, \ldots, N_{\mathbf{t}}$, a subset of the structural responses caused by $\mathbf{F}(t, \boldsymbol{\Theta})$, $\mathbf{Y}_i = [Y_{1,i}(t_i), Y_{2,i}(t_i), \ldots, Y_{M_i,i}(t_i)]^{\mathrm{T}}$, is considered. The elements of $\mathbf{Y}_i$ can be the structural displacement, velocity, or acceleration responses. The response $\mathbf{Y} = [\mathbf{Y}_1^{\mathrm{T}}, \mathbf{Y}_2^{\mathrm{T}}, \ldots, \mathbf{Y}_{N_{\mathbf{t}}}^{\mathrm{T}}]^{\mathrm{T}}$ under a deterministic $\boldsymbol{\theta}$ is jointly Gaussian. The conditional joint PDF of $\mathbf{Y}$ on the condition of $\boldsymbol{\theta}$ is

$$p_{\mathbf{Y}|\boldsymbol{\Theta}}(\mathbf{y} \mid \boldsymbol{\theta}) = \frac{1}{\sqrt{(2\pi)^M D_{\mathbf{Y}}(\boldsymbol{\theta})}}\exp\left[-0.5\mathbf{y}^{\mathrm{T}}\mathbf{R}_{\mathbf{Y}}^{-1}(\boldsymbol{\theta})\mathbf{y}\right], \tag{16}$$

where $\mathbf{y} = [\mathbf{y}_1^{\mathrm{T}}, \mathbf{y}_2^{\mathrm{T}}, \ldots, \mathbf{y}_{N_\mathbf{t}}^{\mathrm{T}}]^{\mathrm{T}}$; $\mathbf{y}_i = [y_{1,i}, y_{2,i}, \ldots, y_{M_i,i}]^{\mathrm{T}}$; $\mathbf{R}_\mathbf{Y}(\boldsymbol{\theta})$ is the covariance matrix of $\mathbf{Y}$, whose elements can be calculated using Eq. (14) with $\mathbf{S}_\mathbf{F}(f_1, f_2, \boldsymbol{\theta})$; $D_\mathbf{Y}(\boldsymbol{\theta})$ is the determinant of $\mathbf{R}_\mathbf{Y}(\boldsymbol{\theta})$; and $M = \sum_{i=1}^{N_\mathbf{t}} M_i$.

The joint PDF of $\mathbf{Y}$ can be calculated by

$$p_\mathbf{Y}(\mathbf{y}) = \int_{\boldsymbol{\Omega}_\boldsymbol{\Theta}} p_{\mathbf{Y}|\boldsymbol{\Theta}}(\mathbf{y} \mid \boldsymbol{\theta}) p_\boldsymbol{\Theta}(\boldsymbol{\theta}) \mathrm{d}\boldsymbol{\theta} = \int_{\boldsymbol{\Omega}_\boldsymbol{\Theta}} \frac{1}{\sqrt{(2\pi)^M D_\mathbf{Y}(\boldsymbol{\theta})}} \exp\left[-0.5\mathbf{y}^{\mathrm{T}} \mathbf{R}_\mathbf{Y}^{-1}(\boldsymbol{\theta}) \mathbf{y}\right] p_\boldsymbol{\Theta}(\boldsymbol{\theta}) \mathrm{d}\boldsymbol{\theta}, \tag{17}$$

where $\boldsymbol{\Omega}_\boldsymbol{\Theta}$ is sample space of $\boldsymbol{\Theta}$ and $p_\boldsymbol{\Theta}(\boldsymbol{\theta})$ is the joint PDF of $\boldsymbol{\Theta}$.

According to Sklar's theorem [38], the joint CDF $P_\boldsymbol{\Theta}(\boldsymbol{\theta})$ of $\boldsymbol{\Theta}$ can be expressed as

$$P_\boldsymbol{\Theta}(\boldsymbol{\theta}) = C_\boldsymbol{\Theta}\left[P_1(\theta_1), P_2(\theta_2), \ldots, P_{N_\boldsymbol{\Theta}}(\theta_{N_\boldsymbol{\Theta}})\right], \tag{18}$$

where $C_\boldsymbol{\Theta}(\boldsymbol{\vartheta})$, $\boldsymbol{\vartheta} = [\vartheta_1, \vartheta_2, \ldots, \vartheta_{N_\boldsymbol{\Theta}}]$, from $[0, 1]^{N_\boldsymbol{\Theta}}$ to $[0, 1]$, is a copula function [38] and $P_i(\theta_i)$ is the marginal CDF of Θ_i, $i = 1, 2, \ldots, N_\boldsymbol{\Theta}$. Then, the joint PDF $p_\boldsymbol{\Theta}(\boldsymbol{\theta})$ is expressed as

$$p_\boldsymbol{\Theta}(\boldsymbol{\theta}) = c_\boldsymbol{\Theta}\left[P_1(\theta_1), P_2(\theta_2), \ldots, P_{N_\boldsymbol{\Theta}}(\theta_{N_\boldsymbol{\Theta}})\right] \prod_{i=1}^{N_\boldsymbol{\Theta}} p_i(\theta_i), \tag{19}$$

where $p_i(\theta_i) = \mathrm{d}P_i(\theta_i)/\mathrm{d}\theta_i$ is the marginal PDF of Θ_i and $c_\boldsymbol{\Theta}(\boldsymbol{\vartheta}) = \partial C_\boldsymbol{\Theta}(\boldsymbol{\vartheta})/\partial\boldsymbol{\vartheta}$. It is assumed that every CDF $P_i(\theta_i)$ has its inverse function

$$\theta_i = P_i^{-1}(\vartheta_i), \tag{20}$$

where $\vartheta_i \in [0, 1]$. Then $p_\mathbf{Y}(\mathbf{y})$ in Eq. (17) can be calculated as

$$\begin{aligned} p_\mathbf{Y}(\mathbf{y}) &= \int_{[0,1]^{N_\boldsymbol{\Theta}}} p_{\mathbf{Y}|\boldsymbol{\Theta}}\left[\mathbf{y} \mid \boldsymbol{\theta}(\boldsymbol{\vartheta})\right] c_\boldsymbol{\Theta}\left(\vartheta_1, \vartheta_2, \ldots, \vartheta_{N_\boldsymbol{\Theta}}\right) \mathrm{d}\boldsymbol{\vartheta} \\ &= \int_{[0,1]^{N_\boldsymbol{\Theta}}} \frac{1}{\sqrt{(2\pi)^M D_\mathbf{Y}\left[\boldsymbol{\theta}(\boldsymbol{\vartheta})\right]}} \exp\left[-0.5\mathbf{y}^{\mathrm{T}} \mathbf{R}_\mathbf{Y}^{-1}\left[\boldsymbol{\theta}(\boldsymbol{\vartheta})\right] \mathbf{y}\right] c_\boldsymbol{\Theta}\left(\vartheta_1, \vartheta_2, \ldots, \vartheta_{N_\boldsymbol{\Theta}}\right) \mathrm{d}\boldsymbol{\vartheta}, \end{aligned} \tag{21}$$

where $\boldsymbol{\theta}(\boldsymbol{\vartheta})$ represents the one-to-one mapping relationships formed by Eq. (20). The integrals in Eqs. (17) and (21) can be numerically computed using the Monte Carlo and quasi-Monte Carlo integrations [39], respectively.

3.2. CDF of the structural extreme response

The Loève spectrum $\mathbf{S}_{\mathbf{F}}(f_1, f_2, \boldsymbol{\theta})$ of the quasi-stationary harmonizable load process $\mathbf{F}(t, \boldsymbol{\theta})$ defined by Eq. (1) is concentrated around the main diagonal line of $f_1 = f_2$ on the dual-frequency plane [22]. Thus, as illustrated in Eq. (12), the Loève spectrum $\mathbf{S}_{\mathbf{U}}(f_1, f_2, \boldsymbol{\theta})$ of $\mathbf{U}(t)$ caused by $\mathbf{F}(t, \boldsymbol{\theta})$ is also concentrated around the main diagonal line on the dual-frequency plane. The Loève spectra of wide-sense stationary processes are exactly lines along the main diagonal line. The similarity between the Loève spectra of the quasi-stationary $\mathbf{U}(t)$ and stationary processes indicates that the out-crossing rate approach [40] can be employed to calculate the extreme distribution of $\mathbf{U}(t)$, which involves replacing the time-invariant second-order statistical moments of stationary processes with the time-varying ones of $\mathbf{U}(t)$. The time-varying moments of $\mathbf{U}(t)$ are also called nongeometric spectral characteristics [14, 41].

The extreme value Y_e of $Y(t)$, which can be a structural displacement, velocity, or acceleration response, over a time duration $[0, T]$ is defined by

$$Y_\mathrm{e} = \max_{t\in[0,T]}\left[\left|Y(t)\right|\right], \tag{22}$$

where $|\bullet|$ is the absolute value operator. The conditional CDF of Y_e given $\boldsymbol{\theta}$ can be approximated as [42]

$$P_{Y_\mathrm{e}|\boldsymbol{\Theta}}(y_\mathrm{e} \,|\, \boldsymbol{\theta}) \approx e^{-N_{Y_\mathrm{e}}(y_\mathrm{e}, T, \boldsymbol{\theta})}, \tag{23}$$

where

$$N_{Y_\mathrm{e}}(y_\mathrm{e}, T, \boldsymbol{\theta}) = \int_0^T \eta_{Y_\mathrm{e}}(y_\mathrm{e}, t, \boldsymbol{\theta})\mathrm{d}t \tag{24}$$

and $\eta_{Y_\mathrm{e}}(y_\mathrm{e}, t, \boldsymbol{\theta})$ is expressed by the Vanmarcke approximation [40, 42]

$$\eta_{Y_\mathrm{e}}(y_\mathrm{e}, t, \boldsymbol{\theta}) = \frac{1}{\pi}\frac{\sigma_{\dot{Y}}(t,\boldsymbol{\theta})}{\sigma_Y(t,\boldsymbol{\theta})}\sqrt{1-\rho_{Y\dot{Y}}^2(t,\boldsymbol{\theta})}\,\frac{1-\exp\left[-\sqrt{0.5\pi}q_Y^{\alpha}(t,\boldsymbol{\theta})\,y_\mathrm{e}/\sigma_Y(t,\boldsymbol{\theta})\right]}{\exp\left[0.5\,y_\mathrm{e}^2/\sigma_Y^2(t,\boldsymbol{\theta})\right]-1}. \tag{25}$$

In Eq. (25), the exponent α of $q_Y(t, \boldsymbol{\theta})$ is taken as $\alpha = 1$ or 1.2 [40]. $\sigma_Y(t, \boldsymbol{\theta})$ is the time-varying standard deviation of $Y(t)$ calculated from its Loève spectrum $S_Y(f_1, f_2, \boldsymbol{\theta})$

$$\sigma_Y(t,\boldsymbol{\theta}) = \sqrt{\int_{-\infty}^{+\infty}\int_{-\infty}^{+\infty} e^{\mathrm{i}2\pi(f_2-f_1)t} S_Y(f_1,f_2,\boldsymbol{\theta})\mathrm{d}f_1\mathrm{d}f_2}. \tag{26}$$

$\sigma_{\dot{Y}}(t, \boldsymbol{\theta})$ is the time-varying standard deviation of the derivative $\dot{Y}(t)$ of $Y(t)$ and can be calculated by

$$\sigma_{\dot{Y}}(t,\boldsymbol{\theta}) = 2\pi\sqrt{\int_{-\infty}^{+\infty}\int_{-\infty}^{+\infty} e^{\mathrm{i}2\pi(f_2-f_1)t} f_1 f_2 S_Y(f_1,f_2,\boldsymbol{\theta})\mathrm{d}f_1\mathrm{d}f_2}. \tag{27}$$

$\rho_{Y\dot{Y}}(t, \boldsymbol{\theta})$, the correlation coefficient of $Y(t)$ and $\dot{Y}(t)$, is defined by

$$\rho_{Y\dot{Y}}(t,\boldsymbol{\theta}) = \frac{r_{Y\dot{Y}}(t,\boldsymbol{\theta})}{\sigma_Y(t,\boldsymbol{\theta})\sigma_{\dot{Y}}(t,\boldsymbol{\theta})}, \tag{28}$$

where $r_{Y\dot{Y}}(t, \boldsymbol{\theta}) = \mathrm{E}[Y^*(t)\dot{Y}(t)]$ is the correlation function between $Y(t)$ and $\dot{Y}(t)$ and can be calculated as

$$r_{Y\dot{Y}}(t,\boldsymbol{\theta}) = \mathrm{i}2\pi\int_{-\infty}^{+\infty}\int_{-\infty}^{+\infty} e^{\mathrm{i}2\pi(f_2-f_1)t} f_2 S_Y(f_1,f_2,\boldsymbol{\theta})\mathrm{d}f_1\mathrm{d}f_2. \tag{29}$$

$q_Y(t, \boldsymbol{\theta})$ is the bandwidth factor of $Y(t)$ and is calculated by

$$q_Y(t,\boldsymbol{\theta}) = \begin{cases} \sqrt{1-\gamma_Y(t,\boldsymbol{\theta})}, & \gamma_Y(t,\boldsymbol{\theta}) < 1 \\ 1-10^{-5}, & \gamma_Y(t,\boldsymbol{\theta}) \geq 1 \end{cases}, \tag{30}$$

where

$$\gamma_Y(t,\boldsymbol{\theta}) = \frac{r_{Y\dot{Y}}^2(t,\boldsymbol{\theta}) + r_{Y\dot{\tilde{Y}}}^2(t,\boldsymbol{\theta})}{\sigma_Y^2(t,\boldsymbol{\theta})\sigma_{\dot{Y}}^2(t,\boldsymbol{\theta})}, \tag{31}$$

and $r_{Y\dot{\tilde{Y}}}(t, \boldsymbol{\theta}) = \mathrm{E}[Y^*(t)\dot{\tilde{Y}}(t)]$. $\dot{\tilde{Y}}(t)$ is the derivative of the auxiliary process $\tilde{Y}(t)$ of $Y(t)$. $r_{Y\dot{\tilde{Y}}}(t, \boldsymbol{\theta})$ is calculated by

$$r_{Y\dot{\tilde{Y}}}(t,\boldsymbol{\theta}) = 2\pi\int_{-\infty}^{+\infty}\int_{-\infty}^{+\infty} e^{\mathrm{i}2\pi(f_2-f_1)t} |f_2| S_Y(f_1,f_2,\boldsymbol{\theta})\mathrm{d}f_1\mathrm{d}f_2. \tag{32}$$

The derivation of Eqs. (30)-(32), as well as that of $\tilde{Y}(t)$ and $\dot{\tilde{Y}}(t)$, is provided in Appendix A.

In [25], a calculation formula of $r_{Y\dot{\tilde{Y}}}(t, \boldsymbol{\theta})$, which is the same as that in Eq. (32), was given. However, the calculation formula of $r_{Y\dot{\tilde{Y}}}(t, \boldsymbol{\theta})$ in [25] was still based on the condition that the target process is characterized by the EPSD. In this study, Eq. (32) is derived from a harmonizable process $Y(t)$. Since the processes characterized by the EPSD belong to the class of harmonizable processes. It is reasonable that the calculation formula of $r_{Y\dot{\tilde{Y}}}(t, \boldsymbol{\theta})$ in Eq. (32) is the same as that in [25].

The CDF of Y_e is approximately calculated as

$$P_{Y_\mathrm{e}}(y_\mathrm{e}) \approx \int_{\boldsymbol{\Omega}_{\boldsymbol{\Theta}}} P_{Y_\mathrm{e}|\boldsymbol{\Theta}}(y_\mathrm{e} \,|\, \boldsymbol{\theta}) p_{\boldsymbol{\Theta}}(\boldsymbol{\theta})\mathrm{d}\boldsymbol{\theta}. \tag{33}$$

Analogy to Eq. (21), $P_{Y_\mathrm{e}}(y_\mathrm{e})$ can be also calculated as

$$P_{Y_\mathrm{e}}(y_\mathrm{e}) \approx \int_{[0,1]^{N_\Theta}} P_{Y_\mathrm{e}|\Theta}\left[y_\mathrm{e} \mid \boldsymbol{\theta}(\boldsymbol{\vartheta})\right] c_\Theta\left(\vartheta_1, \vartheta_2, \ldots, \vartheta_{N_\Theta}\right) \mathrm{d}\boldsymbol{\vartheta}. \tag{34}$$

The integrals in Eqs. (33) and (34) can be numerically computed using the Monte Carlo and quasi-Monte Carlo integrations [39], respectively.

As shown in Eqs. (17), (25), (28) and (31), $\mathbf{R}_\mathrm{s}(\theta)$, $\sigma_Y(t, \theta)$, $\sigma_{\dot{Y}}(t, \theta)$, $r_{Y\dot{Y}}(t, \theta)$, and $r_{Y\dot{\tilde{Y}}}(t, \theta)$ in the time domain are essential for calculating the probability distributions of the structural dynamic and extreme responses. Under the EPSD load model, it has been theoretically proven that these second-order statistical moments may be ambiguous when the loads have time-varying coherences [16]. The ambiguity of the response correlation function under the EPSD load model is numerically verified in Section 4.1. Eqs. (12), (14), (26), (27), (29) and (32) indicate that when the load is modeled as the quasi-stationary harmonizable process, these second-order statistical moments of the structural responses in the time domain can be unambiguously and conveniently calculated using the load Loève spectrum. This is an important advantage of the harmonizable load process model over the EPSD load model. The Gaussian distribution in Eq. (16) and its associated extreme distribution from Eqs. (23)-(25) can be also replaced by other appropriate ones according to various practical applications, which is beyond the scope of this study.

4. Numerical validation

In this section, the efficacy of the proposed approach is validated using two numerical cases. In the first one, a 2-DOF linear elastic structure subjected to a bivariate harmonizable wind speed process with a time-varying coherence is considered. In the second case, a 10-story shear-type linear elastic structure subjected to a harmonizable earthquake ground motion acceleration process is employed. Using the first case, the merit of the harmonizable load process model is highlighted through a comparative analysis with the EPSD load model. The records of all harmonizable load processes considered in this section can be simulated using the simulation method based on the correlation function matrix decomposition [15].

4.1. Case 1

In this subsection, a bivariate zero-mean harmonizable fluctuating wind speed process $\mathbf{u}(t)$ = $[u_1(t),\ u_2(t)]^{\mathrm{T}}$ with a time period of 600 s is applied to a 2- DOF linear elastic structure, as shown in Fig. 1. $U_1(t)$ and $U_2(t)$ represent the displacement responses of the first and second coordinates, respectively, relative to the ground. In this structure, $m = 3 \times 10^6$ kg, $k = 5 \times 10^6$ N/m, and $c = 4 \times 10^5$ N·s/m.

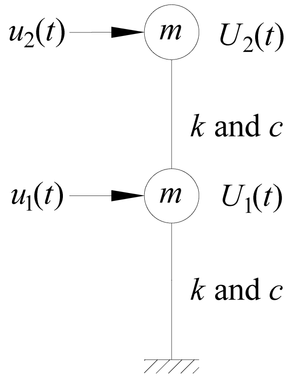

Fig. 1. A 2-DOF linear elastic structure

The WVS matrix $\mathbf{W}_{\mathbf{u}}(t, f, \Theta)$, $\Theta = [\bar{U},\ L_u]$, of the harmonizable wind speed process $\mathbf{u}(t)$ is expressed as

$$\mathbf{W}_{\mathbf{u}}(t,f,\mathbf{\Theta}) = \begin{bmatrix} W_{u_1}(t,f,\mathbf{\Theta}) & r_{\mathbf{u}}(t,f)\sqrt{W_{u_1}(t,f,\mathbf{\Theta})W_{u_2}(t,f,\mathbf{\Theta})} \\ r_{\mathbf{u}}^*(t,f)\sqrt{W_{u_1}(t,f,\mathbf{\Theta})W_{u_2}(t,f,\mathbf{\Theta})} & W_{u_2}(t,f,\mathbf{\Theta}) \end{bmatrix}. \tag{35}$$

In Eq. (35), $\bar{U}$ is the mean wind speed (m/s), L_u is the longitudinal turbulence integral scale (m), $W_{u_1}(t,f,\Theta) = W_{\mathbf{u}}(t,f,\ \bar{U},\ L_u)$ is the auto-WVS of $u_1(t)$, $W_{u_2}(t,f) = W_{\mathbf{u}}(t,f,\ \sqrt{2}\bar{U},\ \sqrt{2}L_u)$ is the auto-WVS of $u_2(t)$, and $W_{\mathbf{u}}(t,f,\ \bar{U},\ L_u)$ is a two-side modulated von Kármán spectrum

$$W_{\mathbf{u}}(t,f,\bar{U},L_u) = A(t)\frac{0.04\bar{U}L_u}{\left[1+70.8\left(fL_u/\bar{U}\right)^2\right]^{5/6}}, \tag{36}$$

where

$$A(t,f) = \exp\left[-2\times10^{-5}(t-300)^2\right]. \tag{37}$$

The time-varying coherence $r_{\mathbf{u}}(t,f)$ in Eq. (35) is expressed as

$$r_{\mathbf{u}}(t,f) = \left[1-5\upsilon(f)\right]e^{ifd(t)-10\upsilon(f)}, \tag{38}$$

where

$$d(t) = 10\sin\left(\frac{\pi t}{300}\right) \tag{39}$$

and

$$\upsilon(f) = \sqrt{0.1f^2 + 10^{-4}}. \tag{40}$$

The Loève spectrum $S_{\mathbf{u}}(f_1, f_2, \bar{U}, L_u)$ of $W_{\mathbf{u}}(t, f, \bar{U}, L_u)$ is

$$S_{\mathbf{u}}(f_1, f_2, \bar{U}, L_u) = \exp\left(-\mathrm{i}600\pi\xi - 5\times10^4\pi^2\xi^2\right)\frac{4\sqrt{5\pi}\bar{U}L_u}{\left[1+70.8\left(fL_u/\bar{U}\right)^2\right]^{5/6}}, \tag{41}$$

where $f = 0.5(f_1 + f_2)$ and $\xi = (f_2 - f_1)$. The correlation function $R_{\mathbf{u}}(t_1, t_2, \bar{U}, L_u)$ of $W_{\mathbf{u}}(t, f, \bar{U}, L_u)$ is

$$R_{\mathbf{u}}(t_1, t_2, \bar{U}, L_u) = A(t)\frac{0.08\sqrt{\pi}\bar{U}L_u\mathrm{K}_{1/3}\left[2\pi|\tau|\Big/\left(\sqrt{70.8}\,L_u/\bar{U}\right)\right]\left(\pi|\tau|\right)^{1/3}}{70.8^{2/3}\Gamma\left(5/6\right)\left(L_u/\bar{U}\right)^{4/3}}, \tag{42}$$

where $t = 0.5(t_1 + t_2)$; $\tau = (t_2 - t_1)$; $\Gamma(\bullet)$ is the Gamma function; and $\mathrm{K}_{1/3}(\bullet)$ is the modified Bessel function of the second kind [43].

In $\mathbf{W}_{\mathbf{u}}(t, f, \mathbf{\Theta})$, the mean wind speed $\bar{U}$ and the longitudinal turbulence integral scale L_u are two correlated random variables. The marginal distribution of $\bar{U}$ is assumed to be a Weibull distribution

$$p_{\bar{U}}(\bar{u}) = \frac{b}{a}\left(\frac{\bar{u}}{a}\right)^{b-1}\exp\left[-\left(\frac{\bar{u}}{a}\right)^{b}\right], \tag{43}$$

where $a = 15$ and $b = 2.5$. The marginal distribution of L_u is assumed to be a lognormal distribution

$$p_{L_u}(l_u) = \frac{1}{l_u\sigma_L\sqrt{2\pi}}\exp\left\{-\frac{\left[\log(l_u) - \mu_L\right]^2}{2\sigma_L^2}\right\}, \tag{44}$$

where $\mu_L = 4$ and $\sigma_L = 0.2$. The probabilistic dependence between $\bar{U}$ and L_u is modeled using a Gaussian copula with a correlation coefficient of 0.7 [44].

The along-wind dynamical force induced by $\mathbf{u}(t)$ is $\mathbf{F}_{\mathbf{u}}(t) = [F_{u_1}(t), F_{u_2}(t)]^{\mathrm{T}}$

$$F_{u_1}(t) = \rho C_D A_T\bar{U}\int_{-\infty}^{+\infty} e^{\mathrm{i}2\pi ft}\chi_{u_1}(f, \bar{U})\mathrm{d}Z_{u_1}(f) \tag{45}$$

and

$$F_{u_2}(t)=\rho C_D A_T\sqrt{2}\bar{U}\int_{-\infty}^{+\infty}e^{\mathrm{i}2\pi ft}\chi_{u_2}(f,\bar{U})\mathrm{d}Z_{u_2}(f), \tag{46}$$

where $Z_{u_i}(f)$ is the frequency component of $u_i(t)$, i = 1 and 2; ρ = 1.225 kg/m^3 is the air density; C_D = 1.2 is the drag coefficient; A_T = 400 m^2 is the tributary area; $\chi_{u_1}(f,\ \bar{U})$ and $\chi_{u_2}(f,\ \bar{U})$ are two aerodynamic admittances [45]

$$\chi_{u_1}(f,\bar{U})=\frac{1}{1+\left(2fA_T^{0.5}/\bar{U}\right)^{\frac{4}{3}}} \tag{47}$$

and

$$\chi_{u_2}(f,\bar{U})=\frac{1}{1+\left[2fA_T^{0.5}\Big/\left(\sqrt{2}\bar{U}\right)\right]^{\frac{4}{3}}}. \tag{48}$$

The wind induced dynamic force $\mathbf{F_u}(t)$ expressed by Eqs. (45) and (46) is also a bivariate harmonizable process and its form is a direct expansion of the stationary wind induced dynamic force [45]. The Loève spectrum $\mathbf{S}_{\mathbf{F_u}}(f_1,\ f_2,\ \boldsymbol{\Theta})$ of $\mathbf{F_u}(t)$ can be calculated by

$$\mathbf{S}_{\mathbf{F_u}}(f_1,f_2,\boldsymbol{\Theta})=\boldsymbol{\chi}(f_1,\bar{U})\mathbf{S_u}(f_1,f_2,\boldsymbol{\Theta})\boldsymbol{\chi}(f_2,\bar{U}), \tag{49}$$

where $\mathbf{S_u}(f_1,\ f_2,\ \boldsymbol{\Theta})$ is the Loève spectrum matrix of $\mathbf{u}(t)$, which can be calculated from $\mathbf{W_u}(t, f, \boldsymbol{\Theta})$; and $\boldsymbol{\chi}(f,\ \bar{U})$ is

$$\boldsymbol{\chi}(f,\bar{U})=\begin{bmatrix}\rho C_D A_T\bar{U}\chi_{u_1}(f,\bar{U}) & 0\\ 0 & \rho C_D A_T\sqrt{2}\bar{U}\chi_{u_2}(f,\bar{U})\end{bmatrix}. \tag{50}$$

The correlation function matrix $\mathbf{R}_{\mathbf{F_u}}(f_1,\ f_2,\ \boldsymbol{\Theta})$ of $\mathbf{F_u}(t)$, which can be computed from $\mathbf{S}_{\mathbf{F_u}}(f_1,\ f_2,\ \boldsymbol{\Theta})$ based on Eq. (5), will be utilized to simulate samples of $\mathbf{F_u}(t)$. In the case of $\bar{U}$ = 20 m/s and L_u = 400 m, $R_{F_1}(t_1,\ t_2)$, $W_{F_1}(t,f)$, and $S_{F_1}(f_1,\ f_2)$ of $F_1(t)$ are illustrated in Fig. 2.

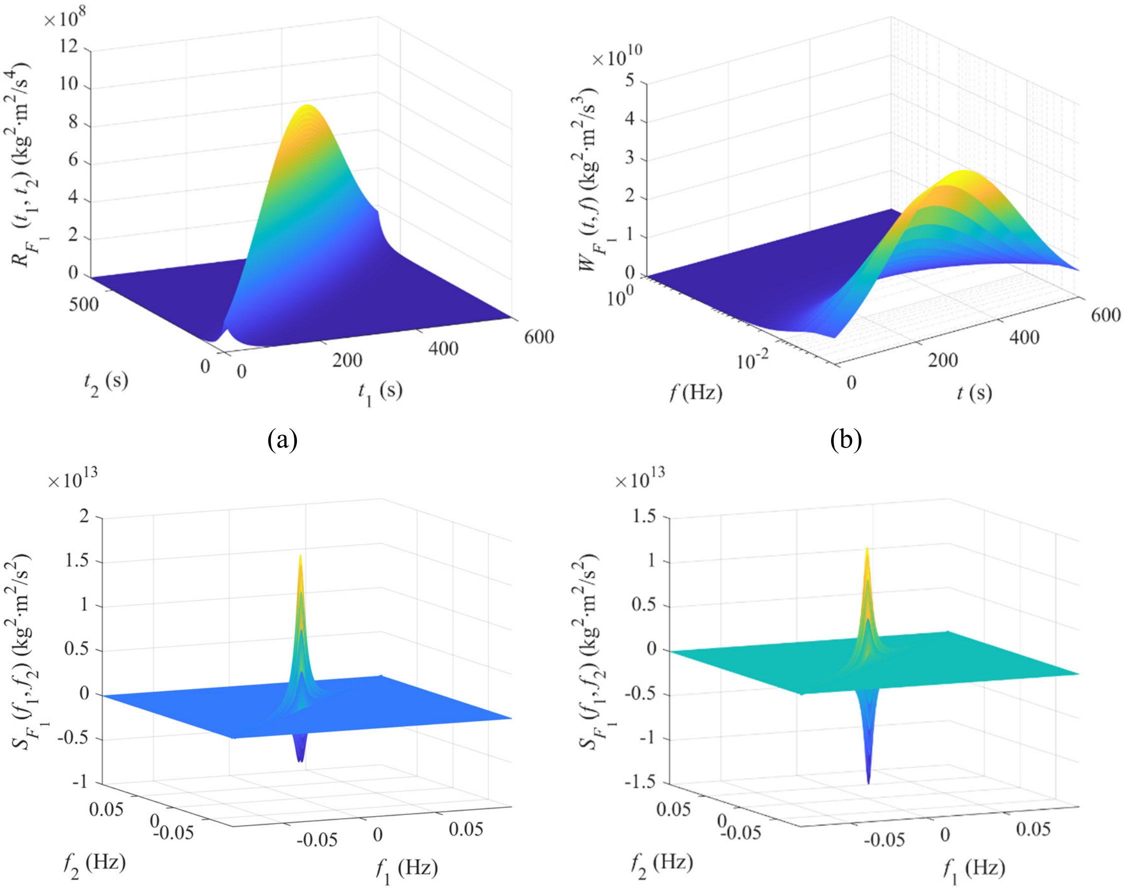

(a) (b)

(c) (d)

Fig. 2. $R_{F_1}(t_1, t_2)$, $W_{F_1}(t, f)$, and $S_{F_1}(f_1, f_2)$ under $\overline{U}$ = 20 m/s and L_u = 400 m. (a) $R_{F_1}(t_1, t_2)$, (b) $W_{F_1}(t, f)$, (c) real part of $S_{F_1}(f_1, f_2)$, and (d) imaginary part of $S_{F_1}(f_1, f_2)$.

In this subsection, following Eqs. (17) and (33), the probability distributions of the dynamic and extreme responses of the 2-DOF linear elastic structure are computed using the Monte Carlo integration [39] with 900 samples of the random physical parameter vector $\mathbf{\Theta} = [\overline{U}, L_u]$. The computed results are then compared with those from 10^6 structural response samples. The response samples are computed using the Newmark method [46] with 10^6 simulated wind force samples.

The evolutionary PDF of the displacement response $U_2(t)$ in Fig. 1, which is computed using Eq. (17), is compared with the result from the response samples, as shown in Fig. 3. It is illustrated that the result from the theoretical formula is consistent with that from the response samples. The CDFs of $U_2(t)$ at t = 200 and 300 s, which are computed by integrating the PDFs computed using Eq. (17), well match the results from the response samples and obviously diverge from their corresponding Gaussian distributions. In Fig. 4, the joint PDF of $U_1(t)$ at t = 400 s and $U_2(t)$ at t = 402 s, which is computed using Eq. (17), is consistent with that from the response samples.

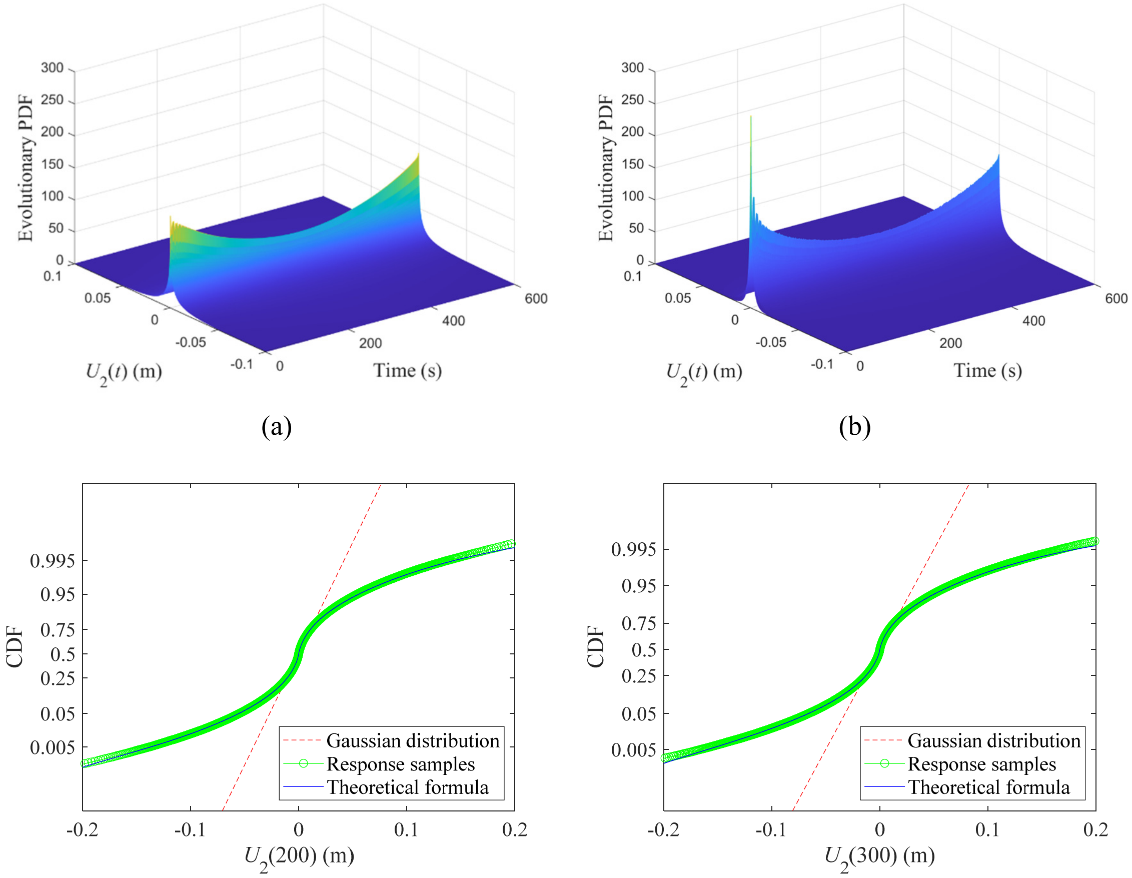

(a) (b)

(c) (d)

Fig. 3. Evolutionary probability distribution of $U_2(t)$. (a) evolutionary PDF calculated using Eq. (17), (b) evolutionary PDF estimated using the response samples, (c) CDF of $U_2(t)$ at $t = 200$ s, and (d) CDF of $U_2(t)$ at $t = 300$ s.

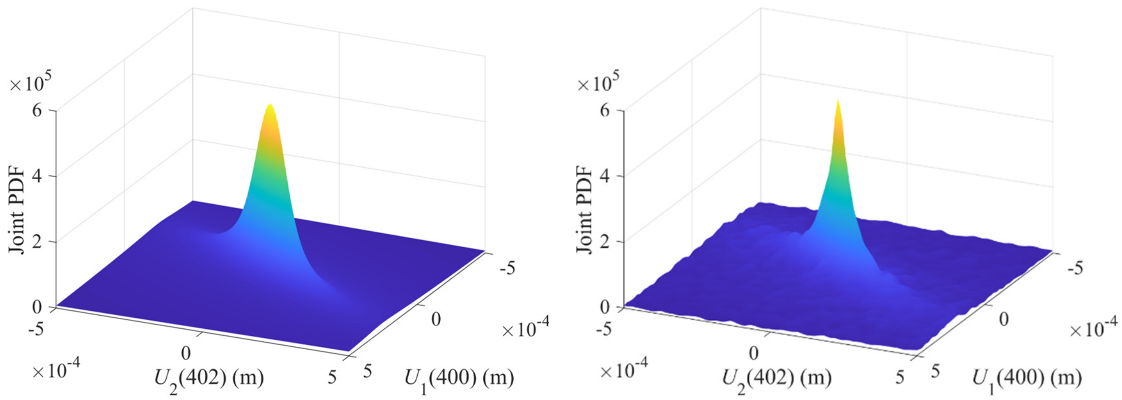

(a) (b)

Fig. 4. Joint PDF of $U_1(400)$ and $U_2(402)$. (a) the result from Eq. (17) and (b) the result from the response samples.

The CDF of $\max(|U_2(t)|)$, the extreme value of $U_2(t)$, is computed using Eq. (33) and compared with the result from the response samples, as shown in Fig. 5. It is illustrated that the extreme distribution of $U_2(t)$ from the theoretical formula well matches the result from the response samples.

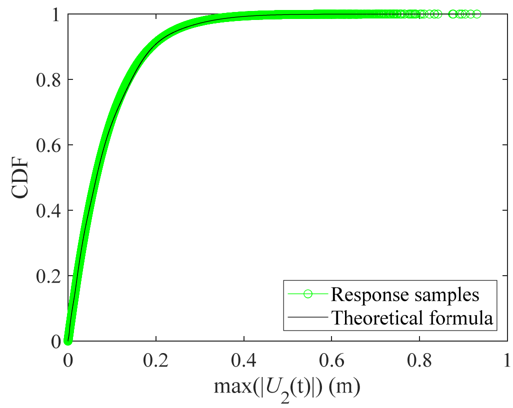

Fig. 5. CDF of max(|$U_2(t)$|).

For the purpose of comparing the EPSD load model and the harmonizable load process model, the bivariate fluctuating wind speed process $\mathbf{u}(t)$ is assumed to be a zero-mean bivariate semi-stationary process [1, 2] and is denoted as $\mathbf{v}(t) = [v_1(t),\ v_2(t)]^{\mathrm{T}}$. The EPSD matrix $\mathbf{P}_{\mathbf{v}}(t, f, \mathbf{\Theta})$ of $\mathbf{v}(t)$ is the same as $\mathbf{W}_{\mathbf{u}}(t, f, \mathbf{\Theta})$ in Eq. (35), that is $\mathbf{P}_{\mathbf{v}}(t, f, \mathbf{\Theta}) = \mathbf{W}_{\mathbf{u}}(t, f, \mathbf{\Theta})$. Then, the evolutionary PDF and time-varying variances of the response displacement response $U_2(t)$ in Fig. 1 caused by $\mathbf{v}(t)$ are computed. The theoretical background for calculating the evolutionary PDF and time-varying variance of $U_2(t)$ under the semi-stationary wind speed process $\mathbf{v}(t)$ is briefly introduced in Appendix B. As illustrated in Eq. (64) in Appendix B, under the semi-stationary wind speed process model involving the time-varying coherence in Eq. (38), the EPSD matrix $\mathbf{P}_{\mathbf{v}}(t, f, \mathbf{\Theta})$ has to be decomposed to obtain $\mathbf{G}_{\mathbf{v}}(t, f)$. In this subsection, the Cholesky decomposition [3] and SRD [16] are employed. Under the semi-stationary wind speed process $\mathbf{v}(t)$, the evolutionary PDFs and time-varying variances of the response displacement response $U_2(t)$ computed using the two matrix decomposition methods are shown in Fig. 6. The same 900 samples of $\mathbf{\Theta} = [\overline{U},\ L_u]$, which are employed to compute the evolutionary PDF of $U_2(t)$ in Fig. 3, are utilized to compute the evolutionary PDFs and time-varying variances of $U_2(t)$ in Fig. 6.

Under the same computational condition, the computation times consumed to compute the evolutionary PDF of $U_2(t)$ employing the harmonizable load process, the EPSD load model with the Cholesky decomposition, and the EPSD load model with SRD are 1.86 hours, 3.29 hours, and 8.98 hours, respectively. The numerical results indicate that the harmonizable load process has a higher computational efficiency than the EPSD load model for this case. Under the EPSD load model, the step of decomposing the EPSD matrix $\mathbf{P}_{\mathbf{v}}(t,\ f,\ \mathbf{\Theta})$ is time-consuming. Moreover, it has been theoretically proven that different matrix decomposition methods can lead to different response correlation functions under the same load EPSD matrix [16]. In Fig. 6(c), it is illustrated that the time-varying variance computed using the Cholesky decomposition is smaller than that using SRD under the same EPSD load model. The difference between the results computed using the Cholesky decomposition and SRD in Fig. 6(c) is apparent, although not large. The time-varying variance of $U_2(t)$ by the harmonizable load process is consistent with that by the EPSD load model with SRD, as illustrated in Fig. 6(c). On the condition of $\overline{U}$ = 5.87 m/s and L_u = 65 m, the time-varying variances of $U_2(t)$ computed using the three methods are displayed in Fig. 6(d). It is shown that the time-varying variance computed using the Cholesky decomposition is obviously smaller than that using SRD. Since the $\overline{U}$ and L_u control the shape of the wind force EPSD matrix, it can be inferred that the ambiguity in the response correlation function caused by different matrix decomposition methods is dependent on the shape of the load EPSD matrix.

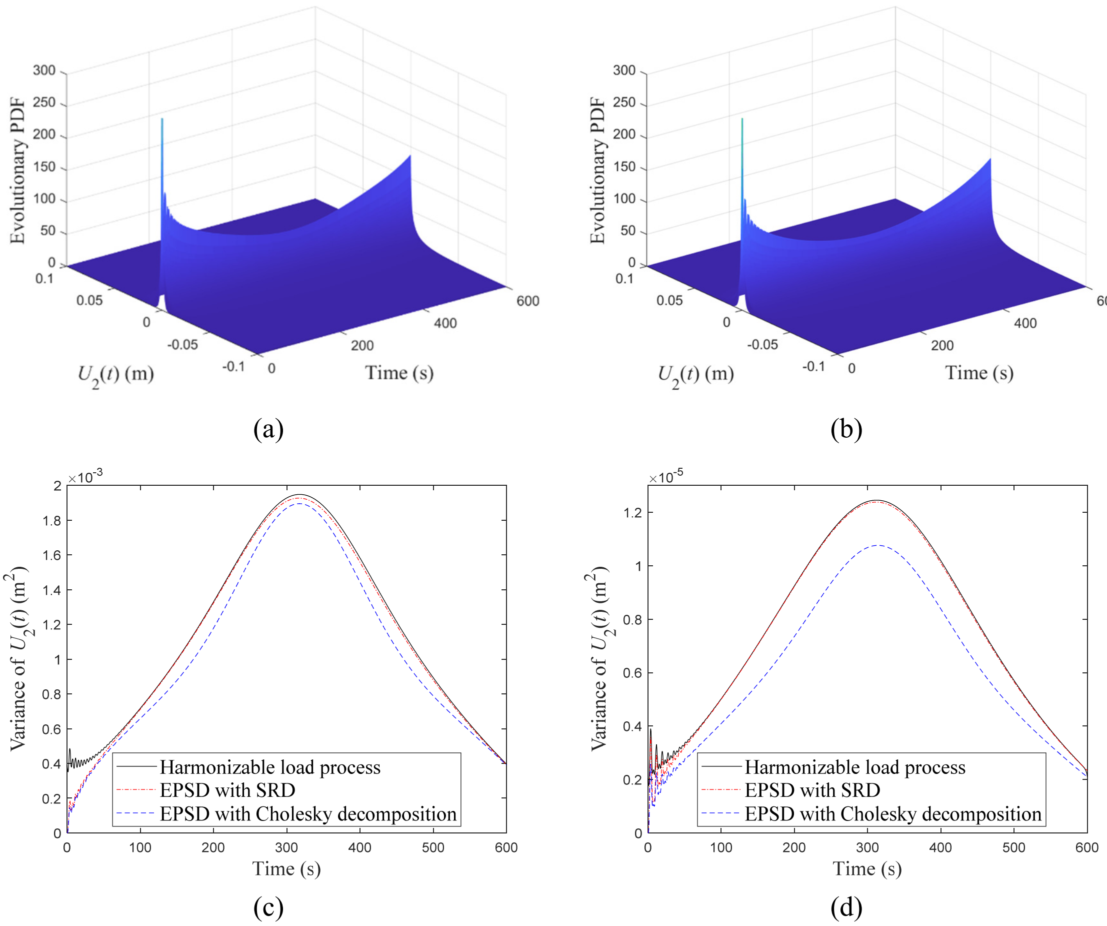

Fig. 6. Evolutionary PDFs and time-varying variances of $U_2(t)$ caused by the bivariate semi-stationary wind speed process $\mathbf{v}(t)$. (a) evolutionary PDF computed with the Cholesky decomposition, (b) evolutionary PDF computed

with the SRD, (c) time-varying variance of $U_2(t)$, and (d) time-varying variance of $U_2(t)$ on the condition of $\overline{U}$ = 5.87 m/s and L_u = 65 m.

4.2. Case 2

In this subsection, an earthquake ground motion acceleration $U_e(t)$ is modeled as a zero-mean quasi-stationary harmonizable process. Its WVS $W_e(t, f, \mathbf{\Theta})$, $\mathbf{\Theta} = [\Theta_1, \Theta_2]$, is [23, 47]

$$W_e(t, f, \mathbf{\Theta}) = \begin{cases} \Theta_1 f^2 t^2 \exp\left[-\Theta_2 (1+f^2) t\right], & t \geq 0 \\ 0, & otherwise \end{cases}, \tag{51}$$

where Θ_1 and Θ_2 are independent random variables. Θ_2 controls the shape of $W_e(t, f, \mathbf{\Theta})$ and it is uniformly distributed in the interval of [0.05,0.15]. Θ_1 controls the magnitude of $W_e(t, f, \mathbf{\Theta})$ and it is assumed to obey a Gamma distribution

$$p_{\Theta_1}(\theta_1) = \theta_1^{\alpha-1} e^{-\beta\theta_1} \beta^{\alpha} / \Gamma(\alpha), \tag{52}$$

where $\alpha = \beta = 2$. The Loève spectrum $S_e(f_1, f_2, \mathbf{\Theta})$ of $U_e(t)$ is [23]

$$S_e(f_1, f_2, \mathbf{\Theta}) = \frac{2\Theta_1 f^2}{\left(f^2+1\right)^3 \Theta_2^3 + 6\mathrm{i}\left(f^2+1\right)^2 \pi\xi\Theta_2^2 - 12\pi^2\xi^2\left(f^2+1\right)\Theta_2 - 8\mathrm{i}\pi^3\xi^3}, \tag{53}$$

where $f = 0.5(f_1 + f_2)$ and $\xi = (f_2 - f_1)$. The correlation function $R_e(t_1, t_2, \mathbf{\Theta})$ of $U_e(t)$ is

$$R_e(t_1, t_2, \mathbf{\Theta}) = \frac{1}{2\Theta_2^{2.5}\sqrt{t}} \exp\left(-\frac{\Theta_2^2 t^2 + \pi^2\tau^2}{\Theta_2 t}\right) \Theta_1 \sqrt{\pi} (-2\pi^2\tau^2 + \Theta_2 t), \tag{54}$$

where $t = 0.5(t_1 + t_2)$; $\tau = (t_2 - t_1)$; and $t_1, t_2 \geq 0$. Fig. 7 illustrates the $R_e(t_1, t_2, \theta)$, $W_e(t, f, \theta)$, and $S_e(f_1, f_2, \theta)$ with $\theta = [1, 0.1]$.

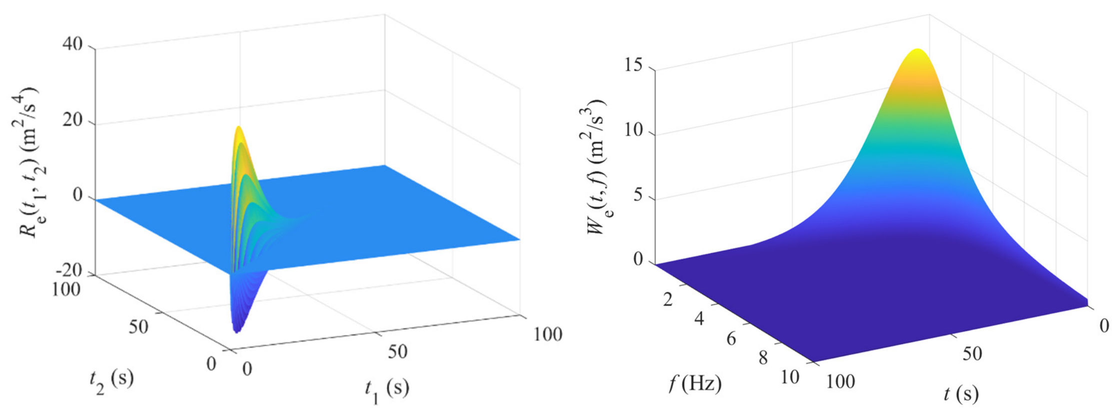

(a) (b)

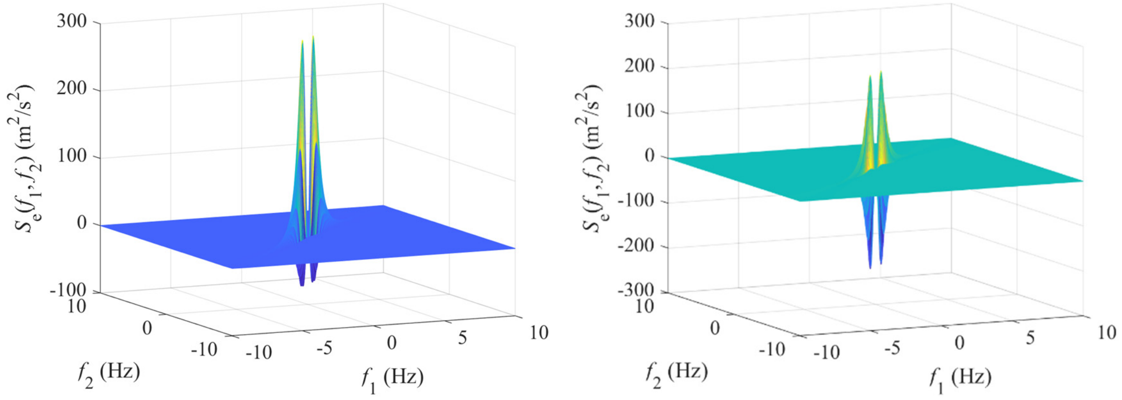

(c) (d)

Fig. 7. $R_e(t_1, t_2, \theta)$, $W_e(t, f, \theta)$, and $S_e(f_1, f_2, \theta)$ under $\theta = [1, 0.1]$. (a) $R_e(t_1, t_2, \theta)$, (b) $W_e(t, f, \theta)$, (c) real part of $S_e(f_1, f_2, \theta)$, and (d) imaginary part of $S_e(f_1, f_2, \theta)$.

A 10-story shear-type linear elastic structure subjected to the earthquake ground motion acceleration $U_e(t)$, as illustrated in Fig. 8, is considered in this study. In the 10-story linear elastic structure, $m = 3.456 \times 10^5$ kg, $k = 1.7 \times 10^8$ N/m, and the damping ratio of its every vibration mode is 0.05. In Fig. 8, $U_i(t)$ represents the displacement response of the i^{th} floor relative to the ground, i = 1, 2,…, 10.

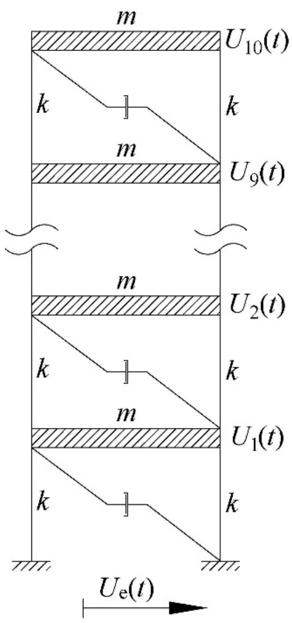

Fig. 8. A 10-story shear-type linear elastic structure

In this subsection, following Eqs. (21) and (34), the probability distributions of the dynamic and extreme responses of the 10-story shear-type linear elastic structure are computed using the quasi-Monte Carlo integration [39] with 200 Sobol points in sample space of $\Theta = [\Theta_1, \Theta_2]$. The computed results are then compared with those from 4×10^4 structural response samples. The response samples are computed using the Newmark method [46] with 4×10^4 simulated earthquake ground motion acceleration samples.

The evolutionary PDF of $U_{10}(t)$, which is computed using Eq. (21), is compared with the result from the response samples, as shown in Fig. 9. It is illustrated that the result from the theoretical formula is consistent with that from the response samples. The CDFs of $U_{10}(t)$ at t = 15 and 60 s, which are computed by integrating the PDFs computed using Eq. (21), are also shown in Fig. 9. The two CDFs from the theoretical formula well match the results from the response samples and obviously diverge from their corresponding Gaussian distributions. The joint PDF of the velocity responses $\dot{U}_5(t)$ at t = 15 s and $\dot{U}_{10}(t)$ at t = 30 s, which is computed using Eq. (21), is compared with the result from the response samples, as illustrated in Fig. 10. The joint PDF computed from the theoretical formula is consistent with that from the response samples.

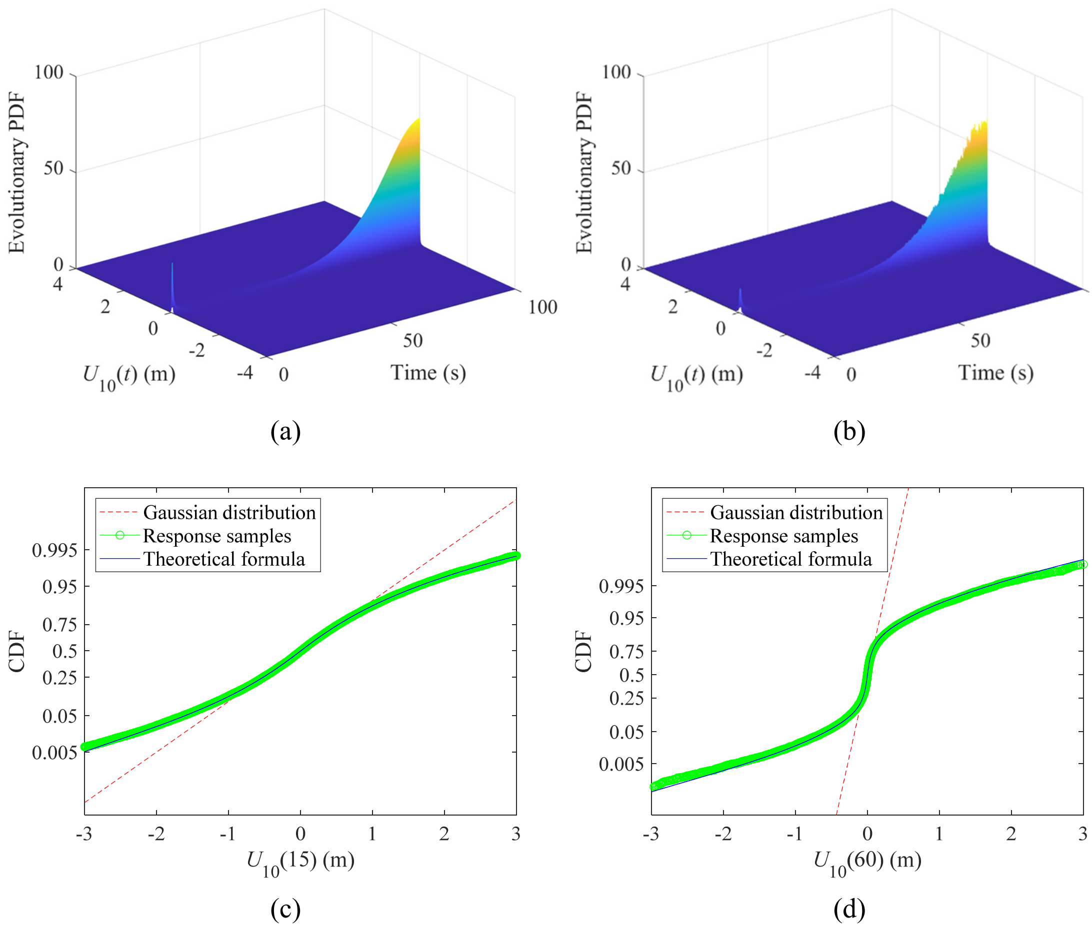

Fig. 9. Evolutionary probability distribution of $U_{10}(t)$. (a) evolutionary PDF computed using Eq. (21), (b) evolutionary PDF estimated using the response samples, (c) CDF of $U_{10}(t)$ at t = 15 s, and (d) CDF of $U_{10}(t)$ at t = 60 s.

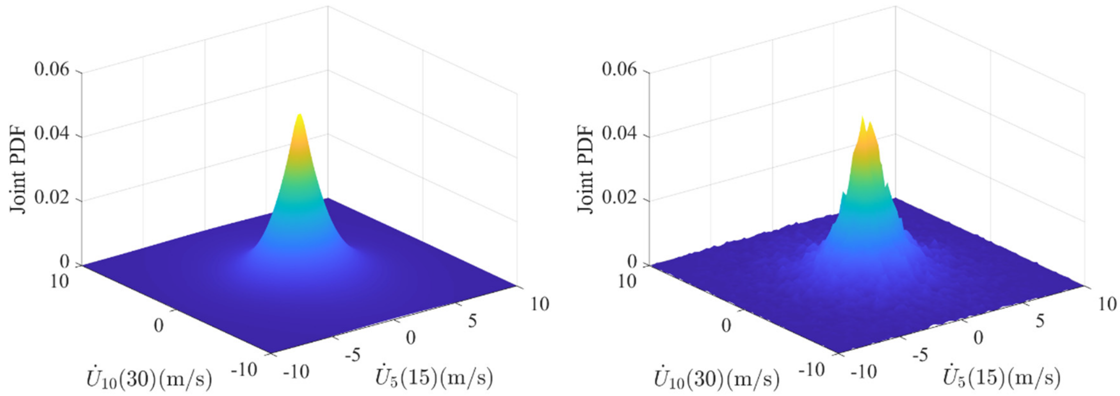

(a) (b)

Fig. 10. Joint PDF of $\dot{U}_5(15)$ and $\dot{U}_{10}(30)$. (a) the result from Eq. (21) and (b) the result from the response samples.

The CDF of the maximum value of the acceleration response $|\ddot{U}_{10}(t)|$, which is computed using Eq. (34), is compared with the result from the response samples, as shown in Fig. 11. It is illustrated that the extreme distribution of $\ddot{U}_{10}(t)$ computed using the theoretical formula well matches the result from the response samples.

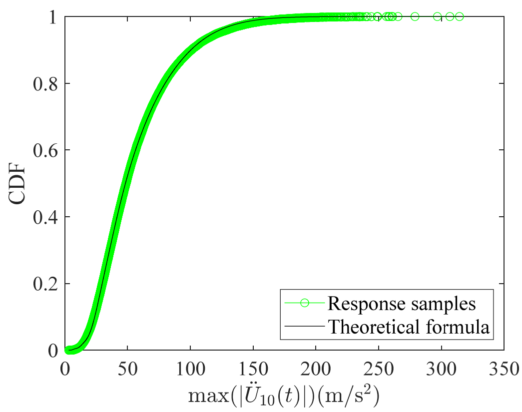

Fig. 11. CDF of $\max(|\ddot{U}_{10}(t)|)$.

5. Conclusions and prospects

In this study, random environmental loads are modeled as quasi-stationary harmonizable processes, with each process characterized by a Loève spectrum containing several random physical parameters. An explicit calculation approach for the dynamics and extreme response probability distributions of a linear elastic structure driven by a quasi-stationary harmonizable load is proposed. Given the values of the load spectral physical parameters, the harmonizable load process is assumed to be Gaussian. The conditional joint PDF of structural dynamic responses at any finite time instants and the conditional CDF of the structural extreme response are expressed in terms of the structural response correlation functions. By multiplying these two conditional probability distributions with the joint PDF of the load spectral parameters, and then integrating these two products over the parameter sample space, the joint PDF of structural dynamic responses at any finite time instants and the CDF of the structural extreme response can be calculated. The efficacy of the proposed approach is numerically verified using two MDOF systems. One is subjected to a bivariate harmonizable wind speed process with a time-varying coherence. The other one is driven by a harmonizable ground motion acceleration process. The numerical results indicate that the probability distributions of structural dynamic and extreme responses computed using the proposed approach are consistent with the results estimated using simulated structural response samples. This validates the feasibility of the proposed approach in analyzing the dynamic and extreme response probability distributions of linear elastic structures subjected to quasi-stationary harmonizable loads. Using the first numerical case, the merit of the harmonizable load process model is highlighted through a comparative analysis with the EPSD load model. The numerical results indicate that the harmonizable load process model has a higher computational efficiency than the EPSD load model for this case. The ambiguity in the response correlation function under the EPSD load model is also verified using this numerical case.

The quasi-stationary harmonizable process has two shortcomings in modeling random loads and analyzing structural responses. First, although the WVS of a harmonizable load process can be assumed to be non-negative, its induced response WVS, which is directly calculated from Eq. (15), may be not non-negative over the entire time-frequency domain. The smoothed WVS with a kernel satisfying certain conditions can be ensured to be non-negative over the entire time-frequency domain, see Sections 5.4 and 5.5 in [48]. This type of smoothed WVSes can be employed to depict the time-frequency distribution of the structural response in cases where the original response WVS (as calculated by Eq. (15)) exhibits negative values. Second, not every non-negative time-frequency function is suitable for representing the load WVS. Considering a non-negative time-frequency function $W(t, f)$ and assuming it to be the WVS of a harmonizable process $X(t)$, its corresponding correlation function $R(t_1, t_2) = \mathrm{E}[X^*(t_1)X(t_2)]$ can be calculated from $W(t, f)$ using a 1D Fourier transform based on Eq. (7). To be a valid correlation function, $R(t_1, t_2)$ must satisfy the condition that

$\sqrt{R(t_1, t_1)R(t_2, t_2)} \geq R(t_1,\ t_2)$ for arbitrary values of t_1 and t_2. Not every non-negative time-frequency function $W(t, f)$ can provide a valid correlation function $R(t_1,\ t_2)$ satisfying this condition. The conditions under which a non-negative time-frequency function can provide a valid correlation function need to be studied in the future.

CRediT authorship contribution statement

Zifeng Huang: Conceptualization, Methodology, Software, Writing-review & editing; **Michael Beer**: Supervision, Project administration.

Declaration of competing interest

The authors declare that they have no known competing financial interests or personal relationships that could have appeared to influence the work reported in this paper.

Acknowledgements

The works described in this paper are financially supported by the Alexander von Humboldt Foundation, to which the authors are most grateful. Any opinions and conclusions presented in this paper are entirely those of the authors.

Appendix A. Derivation of Eqs. (30)-(32)

The response $Y(t)$ caused by the quasi-stationary harmonizable load process $\mathbf{F}(t, \boldsymbol{\theta})$ is also a quasi-stationary harmonizable process and can be expressed as

$$Y(t) = \int_{-\infty}^{+\infty} e^{\mathrm{i}2\pi ft} \mathrm{d}Z_Y(f). \tag{55}$$

The Loève spectrum $S_Y(f_1,\ f_2)$ of $Y(t)$ is defined as

$$S_Y(f_1, f_2) = \mathrm{E}\left[\mathrm{d}Z_Y^*(f_1)\mathrm{d}Z_Y(f_2)\right] \Big/ \mathrm{d}f_1\mathrm{d}f_2. \tag{56}$$

The auxiliary process $\tilde{Y}(t)$ of $Y(t)$ is calculated as

$$\tilde{Y}(t) = -\mathrm{i}\int_{-\infty}^{+\infty} e^{\mathrm{i}2\pi ft} \mathrm{sgn}(f) \mathrm{d}Z_Y(f), \tag{57}$$

where sgn(•) is the signum function

$$\mathrm{sgn}(f)=\begin{cases}1, & f>0\\ 0, & f=0.\\ -1, & f<0\end{cases} \tag{58}$$

The derivative $\dot{\tilde{Y}}(t)$ of $\tilde{Y}(t)$ is calculated as

$$\dot{\tilde{Y}}(t)=2\pi\int_{-\infty}^{+\infty}e^{\mathrm{i}2\pi ft}\left|f\right|\mathrm{d}Z_Y(f). \tag{59}$$

Similar to the stationary process [49], the pre-envelope process $\Psi(t)$ of $Y(t)$ is defined as

$$\Psi(t)=Y(t)+\mathrm{i}\tilde{Y}(t), \tag{60}$$

and the envelope process $V(t)$ of $Y(t)$ is defined as

$$V(t)=\left|\Psi(t)\right|=\sqrt{Y^2(t)+\tilde{Y}^2(t)}. \tag{61}$$

Being quasi-stationary, $S_Y(f_1, f_2)$ of $Y(t)$ is concentrated around the main diagonal line on the dual-frequency plane. In this situation, $r_{Y\tilde{Y}}(t, \boldsymbol{\theta}) = \mathrm{E}[Y^*(t)\tilde{Y}(t)]$ is small and can be approximately assumed to be zero. Under this assumption, the analytical joint PDF of the envelope process and its derivative for a Gaussian non-stationary process, which is given in the Appendix of [41], is also suitable for $V(t)$ in Eq. (61) and its derivative $\dot{V}(t)$. In this situation, the bandwidth $q_Y(t, \boldsymbol{\theta})$ of the harmonizable process $Y(t)$ can be derived from the joint PDF of $V(t)$ and $\dot{V}(t)$ [41] and its calculation formula is given in Eq. (30). $r_{Y\dot{\tilde{Y}}}(t, \boldsymbol{\theta})$ is calculated as

$$\begin{aligned}
r_{Y\dot{\tilde{Y}}}(t,\boldsymbol{\theta}) &= \mathrm{E}\left[Y^*(t)\dot{\tilde{Y}}(t)\right]\\
&=\mathrm{E}\left[\int_{-\infty}^{+\infty}e^{-\mathrm{i}2\pi f_1 t}\mathrm{d}Z_Y^*(f_1)2\pi\int_{-\infty}^{+\infty}e^{\mathrm{i}2\pi f_2 t}\left|f_2\right|\mathrm{d}Z_Y(f_2)\right]\\
&=2\pi\int_{-\infty}^{+\infty}\int_{-\infty}^{+\infty}e^{\mathrm{i}2\pi f_2 t}e^{-\mathrm{i}2\pi f_1 t}\left|f_2\right|\mathrm{E}\left[\mathrm{d}Z_Y^*(f_1)\mathrm{d}Z_Y(f_2)\right]\\
&=2\pi\int_{-\infty}^{+\infty}\int_{-\infty}^{+\infty}e^{\mathrm{i}2\pi(f_2-f_1)t}\left|f_2\right|S_Y(f_1,f_2)\mathrm{d}f_1\mathrm{d}f_2.
\end{aligned} \tag{62}$$

Appendix B. Theoretical background for analyzing $U_2(t)$ under the semi-stationary v(t).

The bivariate semi-stationary wind speed process $\mathbf{v}(t) = [v_1(t),\ v_2(t)]^{\mathrm{T}}$ with a time-varying coherence in Eq. (38) is defined by the Wold-Cramer decomposition [9, 50]

$$\mathbf{v}(t)=\int_{-\infty}^{+\infty}e^{\mathrm{i}2\pi ft}\mathbf{G}_{\mathrm{v}}(t,f,\boldsymbol{\Theta})\mathrm{d}\mathbf{Z}_{\mathrm{v}}(f). \tag{63}$$

In Eq. (63), $\mathbf{Z}_\mathrm{v}(f) = [Z_{1,\mathrm{v}}(f),\ Z_{2,\mathrm{v}}(f)]^\mathrm{T}$ is a complex-valued bivariate zero-mean orthogonal incremental process satisfying $\mathrm{d}\mathbf{Z}_\mathrm{v}^*(-f) = \mathrm{d}\mathbf{Z}_\mathrm{v}(f)$ and $\mathrm{E}[\mathrm{d}\mathbf{Z}_\mathrm{v}^*(f)\mathrm{d}\mathbf{Z}_\mathrm{v}^\mathrm{T}(f)]/\mathrm{d}f = \mathbf{I}$, where $\mathbf{I}$ is an identity matrix. $\mathbf{G}_\mathrm{v}(t,\ f)$ is a complex-valued slowly-varying time- and frequency-dependent modulating function matrix. The EPSD matrix $\mathbf{P}_\mathrm{v}(t, f, \mathbf{\Theta})$ of $\mathbf{v}$(t) is defined as

$$\mathbf{P}_\mathrm{v}(t,f,\mathbf{\Theta}) = \mathrm{E}\left\{\left[\mathbf{G}_\mathrm{v}(t,f,\mathbf{\Theta})\mathrm{d}\mathbf{Z}_\mathrm{v}(f)\right]^*\left[\mathbf{G}_\mathrm{v}(t,f,\mathbf{\Theta})\mathrm{d}\mathbf{Z}_\mathrm{v}(f)\right]^\mathrm{T}\right\} = \mathbf{G}_\mathrm{v}^*(t,f,\mathbf{\Theta})\mathbf{G}_\mathrm{v}^\mathrm{T}(t,f,\mathbf{\Theta}). \quad (64)$$

The along-wind dynamical force $\mathbf{F}_\mathrm{v}(t) = [F_{v_1}(t),\ F_{v_2}(t)]^\mathrm{T}$ induced by $\mathbf{v}(t)$ is calculated as [51]

$$\mathbf{F}_\mathrm{v}(t) = \int_{-\infty}^{+\infty} \boldsymbol{\chi}(f,\bar{U})\mathbf{G}_\mathrm{v}(t,f,\mathbf{\Theta})e^{\mathrm{i}2\pi ft}\mathrm{d}\mathbf{Z}_\mathrm{v}(f), \quad (65)$$

where $\boldsymbol{\chi}(f,\ \bar{U})$ is in Eq. (50).

Given a realization $\boldsymbol{\theta} = [\theta_1,\ \theta_2]$ of $\mathbf{\Theta} = [\bar{U},\ L_u]$, the wind force $\mathbf{F}(t, \boldsymbol{\theta})$ on the condition of $\mathbf{\Theta}$ being $\boldsymbol{\theta}$ is assumed to be a Gaussian process. Under this condition, the displacement response $\mathbf{U}(t)$ of the structure in Fig. 1 caused by $\mathbf{F}(t, \boldsymbol{\theta})$ is Gaussian and can be calculated as [51]

$$\mathbf{U}(t,\boldsymbol{\theta}) = \int_{-\infty}^{+\infty}\mathbf{h}(t-\tau)\mathbf{F}_\mathrm{v}(\tau)\mathrm{d}\tau = \int_{-\infty}^{+\infty}\int_{-\infty}^{+\infty}\mathbf{h}(t-\tau)\boldsymbol{\chi}(f,\theta_1)\mathbf{G}_\mathrm{v}(\tau,f,\boldsymbol{\theta})e^{\mathrm{i}2\pi f\tau}\mathrm{d}\tau\mathrm{d}\mathbf{Z}_\mathrm{v}(f), \quad (66)$$

where θ_1 is the value of $\bar{U}$ and $\mathbf{h}(t)$ is the unit-impulse response function matrix calculated by

$$\mathbf{h}(t) = \int_{-\infty}^{+\infty} e^{-\mathrm{i}2\pi ft}\mathbf{H}(t)\mathrm{d}t \quad (67)$$

and $\mathbf{H}(f)$ is the frequency response function matrix in Eq. (13). The correlation function matrix $\mathbf{R}_\mathrm{U}(t_1, t_2, \boldsymbol{\theta}) = \mathrm{E}[\mathbf{U}^*(t_1)\mathbf{U}^\mathrm{T}(t_2)]$ of $\mathbf{U}(t, \boldsymbol{\theta})$ on the condition of $\mathbf{\Theta} = \boldsymbol{\theta}$ is calculated as

$$\begin{aligned}&\mathbf{R}_\mathrm{U}(t_1,t_2,\boldsymbol{\theta}) \\ &= \int_{-\infty}^{+\infty}\int_{-\infty}^{+\infty}\int_{-\infty}^{+\infty} e^{\mathrm{i}2\pi f(\tau_2-\tau_1)}\mathbf{h}^*(t_1-\tau_1)\boldsymbol{\chi}^*(f,\theta_1)\mathbf{G}_\mathrm{v}^*(\tau_1,f,\boldsymbol{\theta})\mathbf{G}_\mathrm{v}^\mathrm{T}(\tau_2,f,\boldsymbol{\theta})\boldsymbol{\chi}^\mathrm{T}(f,\theta_1)\mathbf{h}^\mathrm{T}(t_2-\tau_2)\mathrm{d}f\mathrm{d}\tau_1\mathrm{d}\tau_2.\end{aligned} \quad (68)$$

Substituting $\mathbf{R}_\mathrm{U}(t_1,\ t_2,\ \boldsymbol{\theta})$ into Eq. (17), the probability distribution of $\mathbf{U}(t)$ at multiple time instants can be calculated.

References

[1] M.B. Priestley, Evolutionary spectra and non-stationary processes, Journal of the Royal Statistical Society: Series B (Methodological), 27 (1965) 204-229.

[2] M.B. Priestley, H. Tong, On the analysis of bivariate non-stationary processes, Journal of the Royal Statistical Society: Series B (Methodological), 35 (1973) 153-166.

[3] G. Deodatis, Non-stationary stochastic vector processes: Seismic ground motion applications, Probabilistic Engineering Mechanics, 11 (1996) 149-167.

[4] J. Chen, F. Kong, Y. Peng, A stochastic harmonic function representation for non-stationary stochastic processes,

Mechanical Systems and Signal Processing, 96 (2017) 31-44.
[5] D. Wang, Z. Fan, S. Hao, D. Zhao, An evolutionary power spectrum model of fully nonstationary seismic ground motion, Soil Dynamics and Earthquake Engineering, 105 (2018) 1-10.
[6] G. Huang, H. Zheng, Y.-l. Xu, Y. Li, Spectrum models for nonstationary extreme winds, Journal of Structural Engineering (ASCE), 141 (2015) 04015010.
[7] A. Kareem, L. Hu, Y. Guo, D.-K. Kwon, Generalized wind loading chain: Time-frequency modeling framework for nonstationary wind effects on structures, Journal of Structural Engineering, 145 (2019) 04019092.
[8] L. Roncallo, G. Solari, An evolutionary power spectral density model of thunderstorm outflows consistent with real-scale time-history records, Journal of Wind Engineering and Industrial Aerodynamics, 203 (2020) 104204.
[9] Z. Huang, Y.-L. Xu, T. Tao, S. Zhan, Time-varying power spectra and coherences of non-stationary typhoon winds, Journal of Wind Engineering and Industrial Aerodynamics, 198 (2020) 104115.
[10] T. Tao, Y.-L. Xu, Z. Huang, S. Zhan, H. Wang, Buffeting analysis of long-span bridges under typhoon winds with time-varying spectra and coherences, Journal of Structural Engineering (ASCE), 146 (2020) 04020255.
[11] G. Muscolino, T. Alderucci, Closed-form solutions for the evolutionary frequency response function of linear systems subjected to separable or non-separable non-stationary stochastic excitations, Probabilistic Engineering Mechanics, 40 (2015) 75-89.
[12] T. Alderucci, G. Muscolino, Fully nonstationary analysis of linear structural systems subjected to multicorrelated stochastic excitations, ASCE-ASME Journal of Risk and Uncertainty in Engineering Systems, Part A: Civil Engineering, 2 (2016) C4015007.
[13] Y. Li, J.P. Conte, M. Barbato, Influence of time-varying frequency content in earthquake ground motions on seismic response of linear elastic systems, Earthquake Engineering & Structural Dynamics, 45 (2016) 1271-1291.
[14] M. Barbato, J.P. Conte, Time-variant reliability analysis of linear elastic systems subjected to fully nonstationary stochastic excitations, Journal of Engineering Mechanics, 141 (2015) 04014173.
[15] F. Yamazaki, M. Shinozuka, Simulation of stochastic fields by statistical preconditioning, Journal of Engineering Mechanics, 116 (1990) 268-287.
[16] Z. Huang, Y.-L. Xu, S. Zhan, Conditionally simulating nonstationary typhoon winds with time-varying coherences for long-span bridges, Journal of Wind Engineering and Industrial Aerodynamics, 212 (2021) 104599.
[17] M. Loeve, Probability theory ii, Springer, 1978.
[18] M.M. Rao, The spectral domain of multivariate harmonizable processes, Proceedings of the National Academy of Sciences of the United States of America, 81 (1984) 4611-4612.
[19] A. Hanssen, Y. Larsen, L.L. Scharf, Complex time-frequency and dual-frequency spectra of harmonizable processes, in: 2004 12th European Signal Processing Conference, Vienna, Austria, 2004, pp. 1577-1580.
[20] P. Flandrin, Time-dependent spectra for non-stationary stochastic processes, in: Time and frequency representation of signals and systems, Springer, 1989, pp. 69-124.
[21] W. Martin, P. Flandrin, Wigner-ville spectral analysis of nonstationary processes, IEEE Transactions on Acoustics, Speech, and Signal Processing, 33 (1985) 1461-1470.
[22] Z. Huang, G. Chen, M. Beer, Multi-taper S-transform method for estimating wigner-ville and loève spectra of quasi-stationary harmonizable processes, Mechanical Systems and Signal Processing, 206 (2024) 110880.
[23] Z. Huang, Y. Xia, Probability distribution estimation for harmonisable loads and responses of linear elastic structures, Probabilistic Engineering Mechanics, 68 (2022) 103258.
[24] A. Chaudhuri, S. Chakraborty, Sensitivity evaluation in seismic reliability analysis of structures, Computer Methods in Applied Mechanics and Engineering, 193 (2004) 59-68.

[25] A. Chaudhuri, S. Chakraborty, Reliability of linear structures with parameter uncertainty under non-stationary earthquake, Structural Safety, 28 (2006) 231-246.
[26] Z. Huang, Y. Xia, M. Gu, G. Fu, Estimating a joint probability distribution model of fluctuating wind speeds of monsoons from field-measured wind speed data, Journal of Wind Engineering and Industrial Aerodynamics, 227 (2022) 105054.
[27] Y. Ding, Y. Peng, J. Li, A stochastic semi-physical model of seismic ground motions in time domain, Journal of Earthquake and Tsunami, 12 (2018) 1850006.
[28] Y. Liu, T. Tao, H. Wang, Z. Xu, Probabilistic turbulence spectra of boundary-layer winds based on measurement at jiangyin bridge site, Journal of Wind Engineering and Industrial Aerodynamics, 231 (2022) 105159.
[29] M. Zhang, J. Zhang, H. Chen, X. Xin, Y. Li, F. Jiang, Probabilistic wind spectrum model based on correlation of wind parameters in mountainous areas: Focusing on von karman spectrum, Journal of Wind Engineering and Industrial Aerodynamics, 234 (2023) 105337.
[30] A. Napolitano, Uncertainty in measurements on spectrally correlated stochastic processes, IEEE Transactions on Information Theory, 49 (2003) 2172-2191.
[31] W. Martin, Time-frequency analysis of random signals, in: ICASSP '82. IEEE International Conference on Acoustics, Speech, and Signal Processing, 1982, pp. 1325-1328.
[32] G.P. Nason, R.V. Sachs, G. Kroisandt, Wavelet processes and adaptive estimation of the evolutionary wavelet spectrum, Journal of the Royal Statistical Society: Series B (Statistical Methodology), 62 (2000) 271-292.
[33] B. Basu, V.K. Gupta, Seismic response of sdof systems by wavelet modeling of nonstationary processes, Journal of Engineering Mechanics, 124 (1998) 1142-1150.
[34] P. Flandrin, On the positivity of the wigner-ville spectrum, Signal Processing, 11 (1986) 187-189.
[35] G. Deodatis, Simulation of ergodic multivariate stochastic processes, Journal of Engineering Mechanics, 122 (1996) 778-787.
[36] M. Shinozuka, C.M. Jan, Digital simulation of random processes and its applications, Journal of Sound and Vibration, 25 (1972) 111-128.
[37] M. Grigoriu, Probabilistic models for stochastic elliptic partial differential equations, Journal of Computational Physics, 229 (2010) 8406-8429.
[38] A. Sklar, Random variables, joint distribution functions, and copulas, Kybernetika, 9 (1973) (449)-460.
[39] G. Leobacher, F. Pillichshammer, Introduction to quasi-monte carlo integration and applications, Springer, 2014.
[40] E.H. Vanmarcke, On the distribution of the first-passage time for normal stationary random processes, Journal of Applied Mechanics, 42 (1975) 215-220.
[41] G. Michaelov, S. Sarkani, L.D. Lutes, Spectral characteristics of nonstationary random processes — a critical review, Structural Safety, 21 (1999) 223-244.
[42] G. Michaelov, L.D. Lutes, S. Sarkani, Extreme value of response to nonstationary excitation, Journal of Engineering Mechanics, 127 (2001) 352-363.
[43] M. Abramowitz, I.A. Stegun, Handbook of mathematical functions: With formulas, graphs, and mathematical tables, Dover Publications, 1965.
[44] H. Joe, Multivariate models and multivariate dependence concepts, CRC Press, 1997.
[45] J.D. Holmes, Wind loading of structures, CRC Press, 2018.
[46] A.K. Chopra, Dynamics of structures, Pearson Education, 2012.
[47] P.D. Spanos, I.A. Kougioumtzoglou, Harmonic wavelets based statistical linearization for response evolutionary power spectrum determination, Probabilistic Engineering Mechanics, 27 (2012) 57-68.

[48] F. Hlawatsch, F. Auger, Time-frequency analysis, John Wiley & Sons, 2013.
[49] M. Di Paola, G. Petrucci, Spectral moments and pre-envelope covariances of nonseparable processes, Journal of Applied Mechanics, 57 (1990) 218-224.
[50] G. Mélard, A.H.-d. Schutter, Contributions to evolutionary spectral theory, Journal of Time Series Analysis, 10 (1989) 41-63.
[51] X. Chen, Analysis of alongwind tall building response to transient nonstationary winds, Journal of Structural Engineering, 134 (2008) 782-791.